

Monitoring hydrological variables from remote sensing and modelling in the Congo River basin

Adrien Paris¹, Stéphane Calmant², Marielle Gosset³, Ayan Fleischmann⁴, Taina Conchy⁵, Jean-Pierre Bricquet⁶, Pierre-André Garambois⁷, Fabrice Papa⁸, Raphael Tshimanga⁹, Georges Gulemvuga Guzanga¹⁰, Vinicius Siqueira⁴, Blaise Tondo¹⁰, Rodrigo Cauduro Dias de Paiva⁴, Joecila Santos da Silva⁵, and Alain Laraque³

¹Ocean Next

²LEGOS-UMR5566 CNES/IRD/CNRS/UPS

³GET-UMR5563 CNRS/IRD/UPS

⁴UFRGS, Instituto de Pesquisas Hidraulicas

⁵Universidade do Estado do Amazonas, RHASA

⁶IRD, HydroSciences Montpellier

⁷INRAE Centre d'Aix en Provence, UMR RECOVER

⁸LEGOS-UMR5566 CNES/IRD/CNRS/UPS; Universidade de Brasilia

⁹Université de Kinshasa, Congo Basin Water Resources Research Center

¹⁰CICOS, Building Kilou, 24 av. Wagania

November 22, 2022

Abstract

This study intends to integrate heterogeneous remote sensing observations and hydrological modelling into a simple framework to monitor hydrological variables in the poorly gauged Congo River basin (CRB). It focuses on the possibility to retrieve effective channel depths and discharges all over the basin in near real time (NRT). First, this paper discusses the complexity of calibrating and validating a hydrologic-hydrodynamic model (namely the MGB model) in the CRB. Next, it provides a twofold methodology for inferring discharge at newly monitored virtual stations (VSs, crossings of a satellite ground track with a water body). It makes use of remotely sensed datasets together with in-situ data to constrain, calibrate and validate the model, and also to build a dataset of stage/discharge rating curves (RCs) at 709 VSs distributed all over the basin. The model was well calibrated at the four gages with recent data (Nash-Sutcliffe Efficiency, $NSE > 0.77$). The satisfactory quality of RCs basin-wide (mean NSE between simulated discharge and rated discharge at VSs, $NSE_{mean} = 0.67$) is an indicator of the overall consistency of discharge simulations even in ungauged upstream sub-basins. This RC dataset provides an unprecedented possibility of NRT monitoring of CRB hydrological state from the current operational satellite altimetry constellation. The discharges estimated at newly monitored locations proved to be consistent with observations. They can be used to increase the temporal sampling of water surface elevation (WSE) monitoring from space with no need for new model runs. The RC located under the fast sampling orbit of the SWOT satellite, to be flown in 2022, will be used to infer daily discharge in major contributors and in the Cuvette Centrale, as soon as data is released.

Monitoring hydrological variables from remote sensing and modelling in the Congo River basin

A. Paris^{1,2,*}, S. Calmant², M. Gosset³, A. Fleischmann⁴, T. Conchy⁵, P.-A. Garambois⁶, J.-P. Bricquet⁷, F. Papa^{2,8}, R. Tshimanga⁹, G. Gulemvuga¹⁰, V. Siqueira⁴, B. Tondo¹⁰, R. Paiva⁴, J. Santos da Silva⁵, A. Laraque³

¹Collecte Localisation Satellites, 11 Rue Hermès, 31420 Ramonville Saint Agne, France.

²IRD / CNES / CNRS / UT, UMR5566 LEGOS, OMP, Toulouse, France.

³IRD / CNRS / CNES / UT, UMR5563 Geosciences Environnement Toulouse OMP, Toulouse, France.

⁴Instituto de Pesquisas Hidraulicas, UFRGS, Porto Alegre, Brazil.

⁵UEA, Manaus, Brazil.

⁶INRAE, UMR RECOVER, Aix-en-Provence, France.

⁷IRD HydroSciences Montpellier, Montpellier, France.

⁸UNB, Universidade de Brasilia, Brasilia, Brazil.

⁹CRREBaC, University of Kinshasa, Kinshasa, DRC.

¹⁰Commission Internationale du bassin Congo-Ubangui-Sangha, Kinshasa, DRC.

*Now at Ocean Next, 90 Chemin du Moulin, 38660, La Terrasse, Grenoble, France.

Corresponding author: Adrien PARIS (adrien.paris@ocean-next.fr)

Key Points:

- The large-scale hydrologic–hydrodynamic MGB model is set-up over the Congo River basin and fed by remote sensing datasets.
- Stage-discharge rating curves are established from simulated discharge and satellite altimetry heights all over the basin.
- For each rating curve, depths and discharges are retrieved routinely from near real time satellite observation.
- In places where the Jason-3, Sentinel3-A or Sentinel3-B virtual stations underlies the 1-day SWOT repeat orbit, it will be possible to infer SWOT discharge as soon as the fast sampling phase begins.

33 Abstract

34 This study intends to integrate heterogeneous remote sensing observations and hydrological
35 modelling into a simple framework to monitor hydrological variables in the poorly gauged Congo
36 River basin (CRB). It focuses on the possibility to retrieve effective channel depths and discharges
37 all over the basin in near real time (NRT). First, this paper discusses the complexity of calibrating
38 and validating a hydrologic–hydrodynamic model (namely the MGB model) in the CRB. Next, it
39 provides a twofold methodology for inferring discharge at newly monitored virtual stations (VSs,
40 crossings of a satellite ground track with a water body). It makes use of remotely sensed datasets
41 together with in-situ data to constrain, calibrate and validate the model, and also to build a dataset
42 of stage/discharge rating curves (RCs) at 709 VSs distributed all over the basin. The model was
43 well calibrated at the four gages with recent data (Nash-Sutcliffe Efficiency, $NSE > 0.77$). The
44 satisfactory quality of RCs basin-wide (mean NSE between simulated discharge and rated
45 discharge at VSs, $NSE_{\text{mean}} = 0.67$) is an indicator of the overall consistency of discharge
46 simulations even in ungauged upstream sub-basins. This RC dataset provides an unprecedented
47 possibility of NRT monitoring of CRB hydrological state from the current operational satellite
48 altimetry constellation. The discharges estimated at newly monitored locations proved to be
49 consistent with observations. They can be used to increase the temporal sampling of water surface
50 elevation (WSE) monitoring from space with no need for new model runs. The RC located under
51 the fast sampling orbit of the SWOT satellite, to be flown in 2022, will be used to infer daily
52 discharge in major contributors and in the Cuvette Centrale, as soon as data is released.

53

54

55

56 1. Introduction

57 Real-time estimates of hydrological variables such as river discharge and stage is of major
58 importance for operational monitoring and informed decision making, with applications to flood
59 control and navigation for instance. Unfortunately, several major basins in Africa suffer from a
60 lack of reliable information to help understanding the hydrological systems and predicting their
61 behaviors. There has been indeed a drastic decrease in daily discharge observation worldwide and
62 particularly in Africa over the last decades [GRDC, 2019]. This lack of information is acute for
63 the Congo River Basin (CRB) for several reasons: the range of scales needed to monitor this large
64 basin [Alsdorf et al., 2016], physiographic features which need to be observed and geopolitical
65 reasons. Also, in a changing climate and under a likely increasing of water stress in central Africa
66 [Schlosser, 2014], it is necessary to improve our capability to measure and understand surface
67 water changes to help mitigate their influence on populations.

68 The CRB is the second largest basin on earth and drains more than 3.7×10^6 km². Despite this
69 major contribution to the world's fresh water cycle, its hydrological behavior is not fully understood
70 yet. The Congo's mean annual flow is around $41.000 \text{ m}^3\text{s}^{-1}$ [Laraque, 2013]. This mean flow is
71 remarkably stable [Spencer et al., 2016], an interesting singularity. Despite its critical importance
72 on local, regional and global water [Hastenrath, 1985] and carbon cycles [Dargie et al., 2017], the
73 CRB has not received as much attention as the Amazon or other large river basins [Alsdorf, 2016].
74 In the CRB, most of people rely on local resources which are strongly impacted by climate change

75 and water availability [Youssoufa Bele, 2013]. Hence, the undergoing climate changes [Mahé and
76 Olivry, 1995; Samba and Nganga, 2012; Nguimalet, 2017; Nguimalet and Orange, 2019] are
77 expected to have severe implications on the populations [Aloysius et al., 2017; Nguimalet and
78 Orange, 2013].

79 To overcome the lack of observational information on the CRB, its behavior has been investigated
80 through hydrological modelling, to analyse global variables such as the continental discharge to
81 the ocean [Syed et al., 2009] or more local phenomena [Tshimanga et al., 2011; Tshimanga and
82 Hughes, 2014, Oloughlin, 2008]. Hydrologic and hydrodynamic modelling has been successfully
83 used in several African basins recently [Logah et al., 2017; Jung et al., 2017; Poméon et al., 2018;
84 Siderius et al., 2018; Getirana et al., 2020; Bogning et al., 2020; Andriambelason et al., 2020] and
85 pointed out as a key tool for flood risk mapping and vulnerability assessment [Eyers et al., 2013].
86 Until now, the lack of comprehensive and distributed measurements in the CRB made it impossible
87 to properly model the discharge and assess its spatial and temporal variability. Some recent studies
88 have attempted to model the entire CRB, but the results show unequal quality and many
89 uncertainties [Chishugi and Alemaw, 2009; BRLi, 2016; Munzimi et al., 2019]. O’Loughlin et al
90 [2020] focused on improving the Congo middle reach hydraulics through hydraulic modelling with
91 hydrological constraints. These studies highlighted the difficulty to set up a hydrological model
92 over a large basin when in-situ discharge data is lacking for proper calibration. They also showed
93 the difficulty to relate recent remote sensing data to hydrological fluxes. This is especially true in
94 complex flow zones like the Cuvette Centrale interfluvial wetlands [Lee et al., 2015] which exhibit
95 superficial laminar runoff qualified as “fluvial table” by Laraque et al. [1998a]. A few studies
96 [Bricquet, 1993; Laraque et al., 2009; BRLi, 2016; Moukandi et al. (this issue)] have however
97 successfully estimated the hydrological balances of the main hydrosystems of the CRB, by
98 combining in situ data from the last century and specific flows using the principle of similarity
99 between a gauged basin and another ungauged neighboring basin with similar physiographic
100 characteristics. Given all these difficulties, remote sensing products, with increasing spatio-
101 temporal resolution over water bodies, represent an interesting source of information to study
102 hydrological responses and balance the lack on in-situ information.

103 Remote sensing products offer a great opportunity for large scale hydrological studies, especially
104 in developing and data-sparse regions [Ekeu-Wei and Blackburn, 2018]. In recent years satellite
105 based precipitation products have reached unprecedented accuracy and precision [Gosset et al.,
106 2018]. Past and current satellite altimetry missions provide reliable information in large ungauged
107 basins [Calmant and Seyler, 2006; Calmant et al., 2008; Seyler et al., 2013] as the CRB. The
108 altimetry data can be used for inferring hydrological variables [Becker et al., 2014; Kim et al.,
109 2019; Carr et al., 2019]. The spatiotemporal variations of surface water storage (SWS) have been
110 mapped thanks to the joint use of satellite altimetry and surface inundation extent [Yuan et al.,
111 2017; Becker et al., 2018]. Hydrological modelling combined with remote sensing datasets has
112 been tested to study the behavior of sever watersheds in Central Africa [Ndehedehe et al., 2017;
113 Fleischmann et al., 2018; Bogning et al., 2020]. Many studies have made use of satellite altimetry,
114 alone or in conjunction with other remote sensing datasets for estimating discharges and/or
115 improving model outputs. Among them, Leon et al [2006], Getirana et al. [2009] and Paris et al.
116 [2016] have estimated rating curves from satellite altimetry and modelled discharges in the Negro
117 basin and in the Amazon basin, respectively. Roux et al [2008], Papa et al. [2010] and Biancamaria
118 et al. [2011] used altimetry measurements together with in-situ limnometric data to produce
119 discharges from satellite. Tarpanelli et al. [2013], Domeneghetti et al [2014] and Garambois et al.

120 [2017] used satellite altimetry to parameterize hydraulic models, which were then used to estimate
121 discharges in ungauged basins [Garambois et al., 2020]. Data assimilation, i.e. the use of
122 observation to correct model states at a given place and at a given time, has also been investigated
123 in the last years in order to improve model outputs, with noteworthy good results in ungauged
124 areas (Paiva et al., [2013a]; Emery et al., [2017]; Revel et al., 2019). Very few of these studies
125 focused on the entire CRB which is a challenging basin because of its scale and the variety of
126 processes to model, and because of the lack of validation data. The forthcoming SWOT mission is
127 expected to provide great opportunities for improving the understanding of large and poorly gauges
128 river systems [Biancamaria et al., 2016]. The SWOT mission lifetime will be split in two
129 sequences: a fast-sampling phase followed by a science phase. During the first phase, SWOT will
130 collect spatially sparser measurements but every day. This phase should allow a comprehensive
131 assessment of SWOT static system parameters for ground processing, errors and uncertainties. The
132 importance of this fast sampling phase is emphasized in the SWOT Cal/Val plan [Chen et al.,
133 2018]. One orbit will cover the CRB during this first daily revisit phase making this basin an area
134 of special interest for the SWOT mission.

135 All the aforementioned studies on the CRB have paved the path for a better understanding of the
136 CRB as a whole basin and specific analysis of some local phenomena and processes [Kim et al.;
137 2017; Carr et al., 2019]. In this study, we intend to bridge the gap between the extensive database
138 collected during the twentieth century and the rich present and future remote sensing datasets. This
139 is achieved through a simple framework based on large scale hydrological modelling and remote
140 sensing datasets for deriving discharges and effective depths in near-real-time all over the CRB.
141 Global and recent remotely-sensed datasets (rainfall from the Global Precipitation Measurement-
142 GPM mission, climatological variables such as pressure, insolation, wind, relative humidity and
143 temperature from CRU, vegetation from ESA-CCI Land Cover, and so on) are used to set up a
144 semi-distributed hydrologic-hydrodynamic model (MGB) and simulate the discharge all over the
145 basin. First, and following Paris et al. [2015], the simulated discharge is used together with satellite
146 altimetry water surface elevations (WSE) to obtain local rating curves over the entire basin. These
147 rating curves are then used to infer discharge and effective depth in near-real time using the latest
148 observations from current satellite altimetry mission. In a second time, the RCs for a given river
149 reach are used to infer a prior of RCs corresponding to new and future missions on the same reach,
150 based on AMHG properties described by Gleason and Smith [2014] and verified in stage/discharge
151 RCs in Paris et al. [2016]. The consistency of such prior discharge is investigated in the light of
152 the few data currently available.

153 2. Datasets and model set-up

154 2.1. Monitoring the CRB from radar altimetry

155 The satellite altimetry data used in this study were obtained from the Jason-2 and 3,
156 ENVISAT, SARAL and Sentinel-3 missions. Their span for the WSE time series are [2002-2010]
157 for ENVISAT, [2008-2016] for Jason-2, [2013-2016] for SARAL, and [2016-today] for Jason3
158 and Sentinel3A missions. Sentinel-3B mission (launched in late 2018) data are also used. For the
159 hydrological modeling set up step, we only considered data in the overlapping period with rainfall

160 estimates, i.e., [2011-2018]. ENVISAT data prior to that period were only considered for the
161 validation of the dataset, and for extending the discharge series into past periods.

162 The WSEs from ENVISAT (ESA) and SARAL (ISRO/CNES) missions were obtained following
163 the methodology presented in Santos da Silva et al. [2010; 2012]. Accordingly, the Icel1 retracker
164 was used to convert the raw radar waveforms into ranges, hence WSE time series, as it was found
165 to provide robust estimates [Frappart et al. 2006, Calmant et al. 2012]. The dataset of virtual
166 stations (VSs) used in the present study is an update of the dataset used by Becker et al. [2014].
167 For the SARAL mission, we extracted a total of 362 VSs (Fig. 01) providing WSE estimates with
168 a 35-day repetition cycle in continuation of the ENVISAT VSs. Following some issues on its
169 guidance system, SARAL was placed on a drifting orbit (4th of July 2016), so that the WSE are not
170 estimated any longer at spatially fixed VSs, but provided in different locations for each orbit –they
171 are still usable and useful, however. For Jason-3 (NASA/CNES) and Sentinel-3A (ESA; hereafter
172 S3A), we used the WSEs freely distributed by the Theia/Hydroweb website
173 (<http://hydroweb.theia-land.fr/>). These time series are obtained by automated processing of the raw
174 radar echoes based on backscatter filtering and outlier detection. All VSs locations are shown on
175 Fig. 01. The Sentinel-3B (hereafter S3B) data, not yet processed by Hydroweb, were manually
176 processed from level2 data retrieved on the Copernicus SciHub (<https://scihub.copernicus.eu/>).

177 The thorough validation of the satellite altimetry dataset (see Appendix A) shows that the WSE
178 time series are globally consistent at the level of few tens of centimeters both in internal (altimetry
179 vs altimetry) and external (altimetry vs gauge readings) comparisons.

180 **2.2. Rainfall estimates from satellite in the CRB**

181 Data availability in the CRB is an issue not only regarding water levels and discharges estimates
182 but also for other variables such as precipitation. Most of in-situ-based datasets provide either
183 mean monthly values or historical series [Alsdorf et al., 2016]. Satellite estimates, especially those
184 based on the GPM constellation, have proved to be a credible alternative to compensate the lack
185 of in-situ data. Some products (namely TRMM TMPA, CMORPH and PERSIANN) have been
186 tested in Beighley et al. [2011]. This study highlighted important discrepancies in the CMORPH
187 and PERSIANN products when comparing with mean annual values from in-situ measurements.
188 Also, the simulated flows having TMPA as input data to a hydrological model had better
189 agreement to discharge records when compared with simulations using CMORPH and
190 PERSIANN inputs. Other recent studies have made use of satellite rainfall estimates in Central
191 African basins with relatively good performances (e.g. Bogning et al. [2020] in the Ogooué basin).

192 In order to make the best use of the current operational altimetry constellation – especially the
193 recent years with the Jason-3 and S3A missions- rainfall estimates covering the last decade are
194 necessary. As the TRMM data is not anymore available since 2016, we used the TAPEER1.5
195 database [Roca et al., 2018] that has been deeply validated against gauges and radar measurements
196 in West Africa [Gosset et al., 2018] and have exhibited good skills in correlation and reproduction
197 of the rain rates frequency distribution. The TAPEER1.5 database provides daily estimates of rain
198 rates in the [2011-2018] period at one-degree resolution.

199 The mean annual rain precipitation estimated over the Ubangui basin, the major right margin
200 Congo River tributary, by TAPEER1.5 are consistent with Mahé et al. [1995] and Bultot et al.

201 [1971], although the study periods differ. The mean annual precipitation rates are respectively of
202 1638, 1529 and 1534 mm. This does not indicate neither a decline nor an increase in precipitation
203 in the last decade in comparison to past periods. In the entire CRB, TAPEER1.5 mean annual
204 rainfall ranges from 1000 mm in the Chambeshi sub-basin (upper Luapula, Zambia) to more than
205 2400 mm for the Maiko, Lowa, Ulindi and Elila sub-basins (see Fig. 02). It is worth noting that
206 these sub-basins are located in the North and South Kivu regions, which are the most lightning-
207 prone regions in the world [Voiland, 2019]. The Cuvette Centrale also receives a large amount of
208 precipitation, with mean annual values higher than 2000 mm. It is hence expected that the
209 precipitation dataset can be used as a valuable input for a hydrologic model to simulate discharges
210 in the CRB.

211 **2.3. MGB model set-up**

212 **2.3.1. Model set-up**

213 MGB is a conceptual, semi-distributed hydrologic–hydrodynamic model developed for tropical
214 regions [Collischonn et al., 2007; Pontes et al., 2017]. It has been extensively applied in large
215 South American basins with low-slope rivers affected by floodplains [Paiva et al, 2013; Siqueira
216 et al., 2018], with some applications also in Africa [Fleischmann et al., 2018]. The model
217 discretizes the basin into irregular unit-catchments and uses the concept of Hydrological Response
218 Units (HRUs) for computation of energy and water budget. MGB was set-up in the CRB using
219 daily TAPEER1.5 precipitation [Roca et al. 2018] for the period of 01/01/2011 to 31/12/2018 and
220 long term climate averages for pressure, mean air temperature, wind speed, sunlight hours and
221 relative humidity from CRU database [New et al., 2002] as the model forcing. These latter
222 variables are used for the computation of evapotranspiration. More detailed information on the
223 internal structure of MGB, hydrologic and hydrodynamics components together with examples of
224 applications can be found in Collischonn et al. [2007], Paiva et al. [2013], Pontes et al. [2017],
225 Fleischmann et al. [2018] and Siqueira et al. [2018].

226 Floodplain topography, as well as basin and sub-basin contours were extracted from the vegetation
227 corrected MERIT DEM [Yamazaki et al., 2017] using the IPH-HydroTools GIS toolkit [Siqueira
228 et al., 2016]. The discretization of the basin led to 32 sub-basins (Fig. 02) and 9920 unit-
229 catchments, the latter having river reaches of equal lengths = 10 km. Bankfull widths (W) and
230 depths (D) were obtained from hydraulic geometry relationships (HG) according to drainage area
231 (A_d) as explained in Paiva et al. [2013]. The HG was considered constant at the sub-basin scale.
232 For each sub-basin, a visual inspection on Landsat images was performed to get the approximate
233 value of W at the outlet and hence derive the HG coefficients. D values for each sub-basin outlet
234 were obtained from historical measurements [Devroey, 1955 and 1956] at the nearest gage (when
235 available) and the HG was applied to the entire sub-basin. When no gage data were available, we
236 kept the HG from the nearest downstream sub-basin. In addition, we manually calibrated W and
237 D values along the Congo River main stream from visual inspection and own knowledge in order
238 to take into account the large short-scale variations of width and depth in this part of the basin,
239 noteworthy for the Stanley Pool and the Livingstone falls. Manning roughness coefficient values
240 were set globally to 0.035.

241 Climatic zones were defined as follow: 1) Northern Hemisphere, 2) Cuvette Centrale, 3) South-
242 Western basins and 4) South-Eastern basins. Following the methodology presented in Siqueira et

243 al. [2018], these zones were considered because of the large dimensions of the basin on either side
244 of the equator, leading to variations in amplitude and time of the variations of albedo and leaf area
245 index (LAI), noteworthy. They encompass the ten zones defined by Bricquet [1993]. HRUs were
246 defined based on the ESA CCI Land Cover for Africa at 20m resolution (available at
247 <http://2016africallandcover20m.esrin.esa.int/download.php>) and on soil profile properties from
248 WoSIS/SoilGrids (available at
249 https://soilgrids.org/#!/?layer=ORCDRC_M_sl2_250m&vector=1) at 250m resolution. This
250 resulted in 12 classes (see Fig. 02). Mean monthly values of albedo and LAI for each HRU and
251 each climatic zone were estimated respectively from the ESA GlobAlbedo project (available at
252 <http://www.GlobAlbedo.org>) at 0.05° resolution and from the ESA Copernicus Global Land
253 Service (available at <https://land.copernicus.eu/global/products/lai>) at 300m resolution.

254 Despite their great importance on local populations and on local and regional climate, and their
255 effective observation from radar altimetry in terms of stage [Cretaux and Birkett, 2006] and in
256 volume [Cretaux et al., 2016], the Tanganyika and Mweru lakes were not properly modelled in
257 this study. Instead, MGB model was forced directly downstream by virtual discharge time series
258 (see hereafter for a description on how such series were obtained). BRLi [2016] evidenced that
259 their influence on the rest of the basin is relatively negligible, and despite their large drainage area,
260 they only contributes to less than 6% of the total runoff at Brazzaville [Bricquet, 1993], somehow
261 comparable in terms of contribution to the Upemba swamps [Charlier, 1955].

262 **2.3.2. Model calibration**

263 Model parameters were manually calibrated against discharge data. As only four gages
264 provide discharge data in the overlapping period [2012 – 2018] (namely Brazzaville/Kinshasa,
265 Ouesso, Bangui, Ilebo), and as these gages are located mainly in the downstream part of the CRB
266 (from the Ubangui to Kinshasa), we decided to build discharge time series from satellite altimetry
267 and historical in-situ information. To do so, we applied the measured rating curves taken from the
268 literature [Charlier, 1955; Devroey, 1958; Magis, 1962; Bergonzini et al., 2015] to WSE time
269 series from nearby VSs at six locations. To convert satellite altimetry heights into gage-compatible
270 stages, we applied an empirical bias to the altimetry estimated so that the rated discharge series
271 fits the mean historical discharge value at the considered VSs. Although discharges estimated in
272 this way may be somehow uncertain, we expect that they provide meaningful information on the
273 water cycle all over the basin and at multi-year time scale, being useful to calibrate model
274 parameters in sub-basins that do not have any recent in-situ discharge measurement. Discharges at
275 Ouesso (Sangha River), Bangui (Ubangui River) and Brazzaville (Congo River) were taken from
276 the SO HYBAM website (freely available at <http://www.so-hybam.org/index.php/eng/>), while
277 CICOS provided the data in the Kasai subbasin. Thanks to the CNES/IRD/AFD/CICOS working
278 group, an extra gage was recently installed at Mbata, in the Lobaye River basin, which is a tributary
279 of the Ubangui River. A rating curve was obtained with Acoustic Doppler Current Profiler (ADCP)
280 measurements, and this gage was also used for model calibration. However, the basin drainage

281 area at this point is much smaller than for the other gages, and consequently its influence on
282 downstream discharges is limited.

283 At each gage, model performance was investigated using the Kling-Gupta efficiency (KGE) and
284 the Nash-Sutcliffe efficiency (NSE), two metrics commonly used in hydrology described in Gupta
285 et al. [2009] and discussed in Knoben et al. [2019].

286 It is commonly agreed that NSE is a more suitable indicator for high flows and KGE for overall
287 performance. The calibration strategy consisted in: 1) manually adapting the width (W) and depth
288 (B) description of the river network in the Congo main stem and 2) modifying the following
289 parameters: W_m , b , K_{bas} , K_{int} , W_c , C_s , CI , C_b at each sub-basin until reaching a good agreement
290 of simulated discharges with gages. The modification of W and B was performed in order to take
291 into account the geomorphologic changes that occur in the main stem, mainly between Kisangani
292 and downstream Kinshasa. For a complete description of the calibration parameters and their role
293 in the hydrology within the model, refer to Collischonn et al. [2007] and Fleischmann et al. [2018].

294 Overall, the model performed very well at simulating daily discharges. When compared to in-situ
295 discharges from gages, the NSE were higher than 0.77 and the KGE higher than 0.81. The
296 comparison with virtual discharges led to more irregular indicators, with mean and median values
297 of 0.54 and 0.50 for NSE, and 0.69 and 0.70 for KGE. NSE and KGE values at all gages considered
298 in this study are provided in Fig. 03. A more detailed analysis of MGB model calibration results
299 can be found in Appendix B together with simulated discharge time series. The values of NSE and
300 KGE globally outperforms those from GW-PITMAN model [Tshimanga and Hughes, 2014]
301 obtained for a longer period but on a monthly basis, and from Munzini et al. [2019] with the
302 GeoSFM model.

303 2.3.3. Model validation

304 As the entire dataset of gage discharges was used for calibration, MGB simulations were validated
305 against independent datasets: flooded areas from several remote sensing sources, WSE from
306 satellite altimetry, and seasonal variability of discharge as reported in the literature. The qualitative
307 (visual) analysis of flooded areas may help to find errors in depth estimates of cross sections. In
308 addition, the validation against water levels fosters a comprehensive assessment of the model
309 performance given the spatial coverage of VSs across the CRB, contributing also to evaluate the
310 consistency of cross-section parameters.

311 2.3.3.1. Simulated water levels

312 The comparison between simulated water levels and WSE from satellite altimetry at *Hydroweb*
313 VSs are presented in Fig. 04. We calculated the Pearson correlation coefficient and the relative
314 variational fraction (ReV), as follows:

$$315 \text{ReV} = \frac{\max(H_{sim}) - \min(H_{sim})}{\max(H_{alt}) - \min(H_{alt})} \quad (1)$$

316 where H_{alt} is the observed satellite altimetry WSE at a given VS and H_{sim} the simulated water
317 level. The optimum value for ReV is 1, and it varies between 0 and $+\infty$. ReV is complementary to
318 the correlation; while the latter provides information on the temporal similarity of the time series,

319 the ReV provides information on the amplitude of variation of the water level at the considered
320 location.

321 In general, there is a satisfactory agreement between the amplitude of variation of the simulated
322 water levels and satellite altimetry, as evidenced in Fig. 04. The mean Pearson correlation
323 coefficient is 0.70, and the median is 0.74. The mean ReV is 0.99, ReV of 80% of the VSs lie in
324 [0.43; 1.86] interval and for 60% of VSs the ReV ranges between 0.56 and 1.28. Some
325 discrepancies were found in the Cuvette Centrale, noteworthy in ungauged sub-basins of the
326 Lulonga River, with ReV values higher than 2. Such discrepancies may indicate an overestimation
327 of the total variation of the water level, probably due to deficiencies in cross section geometry
328 parameterization. It is worth noting that while simulated heights are given at a daily time step,
329 satellite altimetry observations are obtained at an interval of ten to thirty-five days. Therefore,
330 satellite altimetry may not catch all short wavelength variations in water level, and it is expected
331 that the ReV values are globally a little higher than one. Also, as ReV is calculated from max and
332 min of each variable, it is highly impacted by possible outliers. Hence, the proximity of most values
333 with the optimum one indicates that most of the extreme values found in the time series are not
334 outliers. It appears clearly in Fig. 04 that for the Kasai sub-basin the amplitude in simulated water
335 level is lower than the one from satellite altimetry. This is probably due to issues in the [W; B]
336 couples. However, this did not impact the discharge estimates, as the results in this particular sub-
337 basin were satisfactory.

338 2.3.3.2. Flooded areas

339 The CRB is well known for hosting several seasonally or constantly flooded areas [Hughes and
340 Hughes, 1987; Olivry et al., 1989; Laraque et Olivry, 1996], and a good insight on intrinsic model
341 quality can be obtained from the comparison of simulated flooded areas and other datasets. The
342 first region of interest is located in the most upstream part of the basin, on the upper Lualaba and
343 the Luapula Rivers. Much of the region economic activities rely on fisheries [Kolding et al., 2008],
344 and populations are particularly vulnerable to possible impacts of climate change on water
345 availability.

346 The simulated maximum flood extents are presented in Fig.05 for both Bangwelu and Upemba
347 swamps (upper Lwalaba and Luapula, respectively; see Fig. 02 for location), and compared to
348 maximum water extents from the Global Surface Water (GSW; Peckel et al. [2016]), which is
349 based on Landsat optical imagery. Flooded areas simulated by MGB model are in good agreement
350 with GSW. Given the technique adopted, GSW tends to classify only the open waters as flooded
351 waters [Fluet-Chouinard, 2015]. Thus it is expected that other products or even model outputs
352 overestimate flooded areas in comparison with GSW.

353 Results for the central part of the basin show the same behavior as for the upper basin swamps
354 (Fig. 6). However, the model was not able to properly inundate the Cuvette Centrale according to
355 the wetland probability map of Bwangoy et al [2010]. The maximum flooded area from MGB
356 presents an underestimation of flooded area in the Likuala-aux-Herbes / Sangha complex area,
357 while other areas flooding processes seem to be properly modelled. This is probably due to 1) the
358 difficulty of obtaining a DEM with enough accuracy to model short variations of the water surface
359 and under canopy inundation, and 2) a global overestimation of cross section widths or depths in
360 the small reaches of the Cuvette Centrale. Another possible explanation is that some areas are

361 potentially inundated by local rainfall and not by overbank flows [Fleischmann et al., 2020]. That
 362 phenomenon is not represented in MGB model.

363 These two validation methods ensure that the model does not present any severe discrepancies at
 364 remote or ungaged places. Though, Appendix C provides an additional validation of the simulated
 365 discharges through a comparison with flow characteristics such as peak time, flow distribution
 366 among the tributaries and seasonal variability taken from literature and modelling.

367 **3. Rating curves and their applicability for NRT hydrological monitoring from space**

368 In this section, we propose a twofold methodology to derive near real time discharge from satellite
 369 altimetry at both already and newly monitored virtual stations. First, rating curves are estimated at
 370 all the virtual stations with data overlapping the modelled period. These rating curves can now be
 371 routinely used to estimate discharges and depths in near real time. For new and future missions (or
 372 for past missions which operated before the modelled period), it is possible to infer a-priori value
 373 of the RC coefficient, based on the “at many hydraulic geometry” (AMHG) rule [Gleason and
 374 Smith, 2014] considering a well-chosen reach of a given River. From these a-priori coefficients,
 375 one can estimate discharge at any newly monitored location. These steps are described below.

376 **3.1. Rating curves dataset all over the basin**

377 We estimated the rating curve (RC) at each available VS (both from the manually
 378 processed database and from the operational one) using the methodology presented by Paris et al.
 379 [2016]. We excluded the first year of discharges (and the corresponding elevations from altimetry)
 380 to avoid model spin-up issues. A generic RC equation that follows the Manning-Strickler power
 381 law was used (Eq. 02):

$$382 \quad \mathbf{Q}_r = \mathbf{a} \times (\mathbf{H}_{alti} - \mathbf{Z}_0)^b \quad (2)$$

383 where \mathbf{a} , \mathbf{b} and \mathbf{Z}_0 are the three parameters to be optimized, \mathbf{Q}_r is the rated discharge and \mathbf{H}_{alti} is
 384 the WSE from satellite altimetry. The algorithm performs the optimization process while trying to
 385 make \mathbf{Q}_r as similar as possible to \mathbf{Q}_{sim} . More information on the optimization process can be
 386 found in Paris et al. [2016]. In Eq. 01, “a” provides an estimate of the equivalent cross-section
 387 width, Manning’s roughness and water surface slope, while “b” is related to the shape of the cross-
 388 section.

389 When dealing with RCs, the most straightforward analysis is whether or not the discharges
 390 estimated by conversion of WSEs fit the simulated discharges. Fig. 07 provides the spatial
 391 distribution of KGE-based performance between simulated and rating curve-based discharges. We
 392 separated the rating curves into five categories: erroneous and strongly unsatisfactory,
 393 unsatisfactory, intermediate, satisfactory and strongly satisfactory. These categories correspond to
 394 the color code used in Fig. 07, and are limited by the KGE values of 0.25, 0.45, 0.65 and 0.85,
 395 respectively.

396 More than half of the RCs were classified as satisfactory or strongly satisfactory. Only 92 RCs out
 397 of 762 (almost 12%) were classified as erroneous (KGE < 0.2). Those are mainly located over
 398 some small Batekes tributaries (in Congo-Brazzaville) and in the most upstream parts of the
 399 subbasins. This is expected given the difficulties in model calibration due to lack of in-situ gauges.

400 On the other hand, high quality RCs were obtained for other upstream VSs (for instance the
401 Luapula, the Ulindi or the Uele rivers, among others). This suggests that the model was also
402 successfully calibrated for locations with a small contributing area and not only for large
403 tributaries. This is confirmed by the insert in Fig. 7. This insert provides the density of VSs in a
404 given $\log(\text{Ad})$ vs KGE slice. It evidences that the quality of the RCs is not directly function of the
405 drainage area. The RCs with higher quality indicators were obtained for the right margin, Northern
406 Hemisphere tributaries (Ubangui and its tributaries and Sangha), and for the Kasai River. RCs
407 from the Cuvette tributaries also obtained satisfactory overall results.

408 These results must be analyzed with care, as some RCs could present a high quality indicator for
409 the wrong reason. Given the altimetry database used in this study and due to the relatively short
410 run period, some VSs may not offer a large enough number of H/Q pairs to properly evaluate the
411 RCs parameters. Paris et al. [2016] highlighted the link between the number of pairs and the quality
412 of the RC, in terms of both NSE and parameter values. While this is not necessarily an issue for
413 WSE conversion into discharge, this could be problematic for the further use of the RC parameters
414 (see further discussion).

415 If we look back to the Lobaye River at Mbata, we can now compare the measured discharges, the
416 simulated ones and the rated ones (i.e. RC based). These discharges are shown together with the
417 RC in Fig. 8.

418 There is a good agreement between rated and simulated discharges. As expected, as we calibrated
419 the model to fit in-situ discharges, the latter are also close to the rated and simulated ones. The
420 confidence interval is quite large, which is expected as there are few H/Q pairs to be fitted [Paris
421 et al., 2016]. Its size would have been reduced if there were more pairs available.

422 It is worth noting that the RCs differ from one to each other in their possible applications. For
423 instance, the RCs based on SARAL data (ranging from 2013 to 2016) will not be used for real time
424 applications, as the mission was discontinued and the orbit is no longer used. Instead, it can be
425 used for reanalysis of the last decade hydrological behavior of the basin. Indeed, the SARAL
426 mission was placed on the very same orbit as the one from ENVISAT [2002-2010] and from ERS2
427 [1995-2002]. Combining the time series from these satellites and applying to them the RCs derived
428 here, it is possible to obtain long-term time series of discharge. On the other hand, RCs estimated
429 at VSs from Sentinel3-A or Jason-3, currently flying, can be routinely used to infer discharges in
430 near real time, as evidenced hereafter.

431 **3.2. NRT discharges and depths at existent VSs**

432 As the WSEs are delivered in NRT, all RCs extracted over operational VSs enable to infer
433 discharge and depth in NRT. Such an example is provided in Fig. 09 for the Ubangui_Jason_248
434 VS (see Fig. 01 for location). It is worth noting that there are two levels of NRT products, namely
435 the Operational Geophysical Data records (OGDR) and the Interim Geophysical Data Records
436 (IGDR). The OGDR is provided several times a day and within 3 to 5 hours after the satellite
437 overpass, and the IGDR are updated every day and within 1 to 2 days after the satellite overpass.
438 Unlike the OGDR, the IGDR benefits from all the environmental and geophysical corrections,
439 which provide them a better accuracy. The discharge that needed the model to be run (for
440 constructing the RC), and those that are independent of any model run, are represented in purple

441 and green, respectively. An ADCP measurement obtained at 2019-10-26 (peak flow) by Hybam
442 and teams from Bangui University is also displayed for a matter of validation.

443 Fig. 9 shows that the RC was successfully applied to newly acquired data and that the RC-based
444 discharge fits well to the global shape of observed discharges at Bangui (observation 200 km
445 upstream from VS) and is quite consistent to the ADCP record (RMS<10%). This is a very
446 interesting result as far as getting discharges sampled in very high flows is highly uncertain,
447 sometimes leading to inaccurate rated discharge estimation due to extrapolation issues [Paris et al.,
448 2016; Di Baldassarre & Montanari, 2009].

449 3.3. A-priori discharge and depth at newly monitored locations

450 It has been shown that besides providing estimates of depths and discharges, the several
451 RCs estimated along a given reach can also provide useful information on the shape of cross
452 sections [Paris, 2016; Garambois et al., 2017]. Hence, one can use the at-many-stations hydraulic
453 geometry (AMHG) properties along a channel, described by Gleason and Wang [2015] and
454 Gleason and Smith. [2014], and verified for satellite altimetry RCs by Paris et al. [2016], to infer
455 a-priori at-a-station hydraulic geometry (AHG, or the a and b coefficients of the RC) at a single
456 location, such as the newly monitored Sentinel3-B VSs.

457 We checked whether the relationship between a and b is indeed linear in the AMHG space
458 for rivers of the CRB. Fig. 10 provides an insight on the $[a, b]$ relationships for Ubangui, Kasai,
459 Sangha and Congo rivers. It is worth noting that the coefficients that are investigated are not
460 directly the a and b coefficients, but c and f from $d = c * Q^f$ [Gleason and Smith, 2014]. A simple
461 transformation into the rating curve equation (Eq. 01) led to the relationships $f = \frac{1}{b}$ and $c = \frac{1}{af}$,
462 that are show in Fig. 10.

463 For these four Rivers, we only considered the main channel VSs, i.e. from the river mouth until it
464 splits into a major tributary. We excluded the $[f, c]$ pairs with b coefficient lower than 1.1 because,
465 according to Paris et al. [2016] such pairs are commonly found at VSs with erroneous RC (either
466 because the mathematical formulation adopted in this study is not suited to this specific RT or
467 because of the insufficient quality of one of the H and Q series). We also excluded those with
468 KGE lower than 0.70. It is evidenced in Fig. 10 that the a and b coefficients do follow a linear
469 relationship, with correlations higher than 0.90 for the four river reaches studied. The Oubangui,
470 Sangha and Congo Middle reach present $[f, c]$ pairs well distributed in the domain, while the
471 Aruwimi River RCs (hexagrams) are more constrained in a reduced zone. This is possibly due to
472 a more constant geometry in the Aruwimi River or to a reduced number of tributaries, leading to
473 less changes in the RC coefficients.

474 It is interesting to note that the AMHG relationship provides an additional tool for validation the
475 RCs. As a matter of fact, those RCs with problematic coefficients values or lower quality are
476 clearly identifiable in the AMHG space (see the crosses in Fig. 10). Once the $[a, b]$ relationship is
477 found, it is possible to infer the value of this pair for each location between the most downstream
478 and most upstream VSs used. To do so, the slope and the intersection of the line is estimated. It is
479 worth remembering that a proxy for the RC coefficient a at a given location is given by:

$$480 \quad \mathbf{a} = \frac{\mathbf{w} \times \sqrt{s}}{n} \quad (6)$$

481 where W is the width of the equivalent rectangular cross section in Manning's simplification, n is
 482 the Manning roughness coefficient and s is the water surface slope.

483 For each VS, the Manning's roughness can be fixed at 0.035, as it was in the model
 484 parameterization, since no better alternate value is known. At a given VS, the width (W) can be
 485 either estimated from a Google Earth imagery visual inspection, or using GWD-LR database
 486 [Yamazaki et al., 2014], the global dataset from Andreadis et al. [2013], or GRWL [Allen and
 487 Pavelski, 2018]. For the slope, we used the mean WSE profile from multi-mission satellite
 488 altimetry levels forced by the MERIT DEM [Yamazaki et al., 2017].

489 We built a longitudinal profile of each river reach in the basin using both satellite altimetry and
 490 the MERIT DEM [Yamazaki et al., 2017]. The estimated profile of the Congo River is given in
 491 Fig. 11. Fig. 11 also provides the validation of this profile against an ADCP measurement from
 492 the CRUHM projet (CRuHM, 2018). Thanks to this profile we also derived the predicted Z_0
 493 parameter (cease-to-flow height at the considered VS). To do so, the Z_0 parameter was
 494 extrapolated between each VS by a function following the longitudinal profile. Fig. 11 evidences
 495 that at the location of the measurement, the estimated Z_0 is consistent with the median depth of
 496 the ADCP profile of cross section. The parameter values and RC coefficients extrapolated at VS
 497 Sentinel3-B pass 541 are presented in Table 01.

498 We extracted manually the time series of WSE from raw data of the Sentinel3-B mission at the VS
 499 from the pass 541 (see Fig. 01 for location). This VS is located in the Congo River main stem,
 500 downstream of Kisangani. It also lies under the SWOT 1-day repeat orbit, near a S3-A crossover
 501 and in the vicinity of a gage (namely Bumba), as evidenced in Fig. 12 (upper panel). At this VS,
 502 we estimated the width as 4000 m. Using the value of 0.035 for Manning's roughness coefficient
 503 and the value of 0.047 m.km^{-1} for the slope (value given by the longitudinal profile) we get a value
 504 of 695 for the coefficient a . The interpolation of the Z_0 s from previously processed VSs led to a
 505 Z_0 value of 352.05 m. We then applied the regression rule for the Congo River (Fig. 10) and get
 506 the value of 1.864 for the b coefficient.

507 We now have all the needed coefficient to convert the newly released Sentinel3-B VS time series
 508 into discharges through the estimated rating curve. The discharge time series is provided in Fig.12.

509 It is evidenced in Fig. 12 that the transformation provided a globally satisfactory estimate of
 510 discharge at this newly monitored VS. It is not straightforward to infer how accurate this discharge
 511 is, as no validation is possible against in-situ discharge, and we did not simulated discharges on
 512 this period either. One possible validation is by comparison of estimated discharges and other rated
 513 discharges. The discharges estimated at S3-B VS are consistent with those from Jason-3 and
 514 Sentinel3-A missions in the same period, although the peak flow seems slightly overestimated.
 515 However, it has recently been acknowledged in newspapers that the Congo is facing one of the
 516 worst flood in the last decades [Boko, 2019], and the discharge value found at highest point (around
 517 $25,000 \text{ m}^3\text{s}^{-1}$) is consistent with this assertion. Also, the remarkable 2017 drought evidenced on
 518 the discharge at Brazzaville/Kinshasa is well represented on the altimetric discharges time series.
 519 The consistency of the altimetric discharges is also evidenced by the comparison to Kisangani
 520 gaged discharge. The rated discharges from Jason-2 observations present a mean difference to
 521 those at Kisangani of $4400 \text{ m}^3 \text{ s}^{-1}$ on the [2008 – 2012] period and the hydrological cycle is well
 522 caught. Kisangani is located 300 km upstream Bumba and on this reach rivers as the Lindi, the

523 Lomami and the Aruwimi increases the discharge by $4600 \text{ m}^3\text{s}^{-1}$ per year [Rodier, 1983]. This
524 seems to confirm the validity of the rated Jason discharges, and consequently the consistency of
525 the S3-B discharges obtained from the AMHG properties. It is worth noting that the discharge
526 derived from such AMHG relationship is strongly dependent on the estimated Z_0 . Indeed, a brutal
527 change in bathymetry (e.g. falls or pools) may lead to overestimation (respectively
528 underestimation) of the discharge if such change was not properly observed neither from altimetry
529 nor in the DEM and if the Z_0 is underestimated (respectively overestimated).

530 This method can be used for any newly monitored location (e.g., any new mission) provided that
531 RCs have been previously computed both upstream and downstream of such location. This
532 increases consequently the a priori database that can be made available to scientific teams before
533 the launch of SWOT. This also increases the temporal sampling of any given reach of the rivers
534 with no need for a new model run.

535 4. discussion and conclusions

536 This study was conducted in order to provide a simple framework for NRT discharge
537 estimates from satellite altimetry in the CRB. To do so, MGB hydrologic–hydrodynamic model
538 was set up and run with the GPM TAPEER1.5 daily precipitation product as entry. The model was
539 calibrated against a series of observed discharge that combined i) few in-situ gages available on
540 the overlapping period [2012-2018], and ii) discharge time series computed from satellite
541 altimetry water levels and previously established rating curves. Only part of the WSE dataset was
542 used for calibration purposes in order to keep an independent time series for validation. A more
543 extended dataset of in-situ measurements and surveyed cross sections (i.e., information on bankfull
544 width and depth) would have been useful for the set up and calibration of the model, but was not
545 available. The model was validated in terms of discharge, water level and flooded areas by
546 independent datasets and historic information. Globally the model outputs showed good
547 consistency with observations, although we observed a potential lack of inundation in the Cuvette
548 Centrale region. The issue of the Mweru and Tanganyika great lakes was addressed by Hughes et
549 al. [2013] and Tshimanga and Hughes [2014]. Our study could benefit from a similar approach.
550 Overall, the model simulated discharges compare well with observation, MGB outperforming
551 other hydrological models previously applied in CRB. For future studies the flooded areas in the
552 flattest areas (Cuvette Centrale, Bangwelu swamps, etc.) could benefit from the 2D connections
553 recommended in recent studies [Hoch et al., 2017; Fleischmann et al., 2018] and also from finer
554 resolution DEMs. This is also the very first time that the TAPEER1.5 precipitation product is
555 applied for hydrological applications in central Africa, showing its adequation for such use. This
556 opens the way for more extensive use of the proposed combined approach that uses hydrological
557 modeling with an ensemble of satellite data, in African poorly-gauged and ungauged basins.

558 We extensively validated the satellite altimetry WSE dataset (in part an extension of the dataset
559 presented by Becker et al. [2014]) with both internal and external comparisons. At the 1.5-day
560 crossings, the accuracy is better than 0.40 m for ENVISAT and 0.25 m for SARAL. This validation
561 was complemented with an external validation with past chronicle of monthly values, revealing an
562 accuracy better than 0.30 m. For the operational satellite altimetry constellation, the accuracy is
563 better and up to 0.10 m, as evidenced by the comparison with recently installed gages. By pairing
564 these WSE with simulated discharges, we built a unique rating curve dataset using the
565 methodology from Paris et al. [2016] and a simple power law equation. The quality indicators

566 associated with Paris et al (2016) method are globally very high for the CRB, with median ENS
567 and KGE values of 0.68 and 0.74, respectively. This means the proposed method reaches a robust
568 and consistent solution over most of the CRB. For some VSs however, despite the high ENS, the
569 retrieved RC coefficient are out of the expected range and the solution is unsatisfactory. It was the
570 case, for instance, for several VSs from Saral/AltiKa observations because of the very few H/Q
571 pairs available. These VSs could however still be used for estimating long term time series of
572 discharge from satellite altimetry using the records from ERS2, ENVISAT and SARAL missions.
573 These discharge series could be then assimilated in partially calibrated hydrological models to
574 improve the spatial characterization of flows along the basin. This could help understanding some
575 of the specific processes that occur in the Cuvette Centrale and the carbon exchanges across the
576 CRB. All the rating curves estimated from Jason and Sentinel-3 measurements can now be
577 routinely used for NRT applications, such as monitoring water availability in the basin and even
578 navigation guidance, especially at the operational VSs where agencies are committed to provide
579 data for several years. This database will also be of great importance for preparing the a priori
580 datasets for the forthcoming SWOT mission.

581 An estimate of surface slope and bathymetry was obtained using the WSE database, the Z0
582 coefficients from the RCs and an interpolation between the VSs forced by the MERIT DEM
583 [Yamazaki et al., 2017]. We then used the rivers AMHG properties to infer synthetic RCs at
584 ungauged locations. We applied this methodology at a Sentinel3-B VS lying under the 1-day repeat
585 orbit of the SWOT mission. The comparison with the rated discharges obtained at other VSs
586 proved the consistency of this first guess RCs. Unfortunately, we were unable to directly compare
587 it with in-situ data as there is no information currently available near this location for 2019. The
588 validation was performed through the comparison of rated discharge and in-situ discharge on a
589 past period. This site is of huge interest as it concentrates in few kilometers and under the SWOT
590 fast sampling orbit two S3B crossovers (one under each swath), one S3A crossover and one in-
591 situ gage at Bumba waterway port. At this site, and thanks to the now already processed rating
592 curves, it will possible to infer SWOT discharge as soon as the fast sampling phase begins, while
593 the release of the official products will take a few months. This is why this site should be
594 considered as a gold site for the SWOT Cal/Val and receive a particular attention from agencies.
595 Also, we are now confident that it is possible to infer an a priori value of discharge at any location
596 located within the frame of our initial VSs dataset. Moreover, we are able to identify erroneous
597 RCs to be disregarded in the dataset. This is particularly useful for the now flying Sentinel3-B
598 mission that should provide in the very short term around 500 VSs distributed in the CRB. This
599 new data set will increase the number of daily observations over the CRB from satellite altimetry
600 from almost 20 to more than 40, with no need for new model runs. We believe this information
601 will be useful for a better understanding and monitoring of the hydrological processes in the CRB,
602 and that it will contribute to improve the error budget of the Congo total flows going into the
603 oceans.

604

605 **Acknowledgements:**

606 Authors would like to acknowledge the French space agency CNES for financial support. Authors
607 also gratefully acknowledge the CICOS and its members for their efforts in collecting and
608 providing valuable data. This study was made possible thanks to SO/HYBAM data. Water surface

609 elevation time series were collected from the Theia/Hydroweb website ([http://hydroweb.theia-](http://hydroweb.theia-land.fr/)
610 [land.fr/](http://hydroweb.theia-land.fr/)). Authors also gratefully acknowledge the RHASA laboratory for manual processing of
611 raw altimetry data, extracted from the database maintained at CTOH/LEGOS
612 (<http://ctoh.legos.obs-mip.fr/>)

613
614**Appendix A: Satellite altimetry database validation**

615 This appendix intend to provide a direct analysis of the altimetric data temporality and
616 accuracy through an extensive validation of WSE time series. As evidenced in Fig. 01, the VSs
617 database provides a good sampling of the entire basin, with 55 tributaries being sampled by at least
618 one VS. When possible, the dataset is compared to in-situ gages on the overlapping period, and
619 additional validation is performed by means of comparison of seasonal cycles of WSE with gage
620 data from the 1940 – 1960 period, and by comparison between altimetry series. In CRB, some
621 ENVISAT/SARAL ground tracks make crossings at 1.5 day time interval. This means that in less
622 than two days the satellite overflies the –almost- same location twice. Following Silva et al. [2010],
623 we made the hypothesis that the difference between two estimates of WSE in a 1.5 days interval
624 could be used as a proxy of the measurement error, i.e. that the considered river flow is stationary
625 on 1.5 day. The location of the 24 crossings selected for this analysis is presented on Fig. A1a. 15
626 rivers are included in this dataset, with reach width ranging from 30 m to 4 km. 90% of the
627 differences are below 25 (40) cm for SARAL (ENVISAT). The histogram can be found on Fig.
628 A1b.

629 In order to enlarge the validation of our WSE dataset, we also compared it with archive series.
630 Altimetry monthly averages were compared with the monthly average of ancient in-situ series in
631 neighbor reaches. Stage series for 19 stations were provided by the international commission of
632 the Congo-Ubangui-Sangha basin (CICOS). We selected 16 of these stations with distance less
633 than 50 km from the corresponding VS. Long term averages were removed from all gauges and
634 VSs monthly series before comparison, and the global RMSE between them is 0.32 m (Figure A2).
635 The fit between VSs and gauges is highly variable. In some cases, the actual WSE climatology at
636 VS fits well the ancient gauge climatology, as for example in the case of Bagata on the Kwilu
637 River (RMS difference 9 cm), or Ilebo on the Kasai river (RMS of 10 and 14 cm). The lowest
638 performance is observed for Basoko on the Congo River where RMS difference is larger than 60
639 cm. Many factors besides errors in the altimetry series may explain the difference between the
640 chronicles, such as change in the hydrological functioning of the upstream basins or of the local
641 river morphology, errors in the gauge series, etc. Hence, the figures provided hereafter
642 overestimate the error in the altimetry series and we can assess that the latter provide mean monthly
643 water level at the accuracy level of 30 cm.

644

Appendix B: MGB model calibration results

645 Comparisons between simulated and in-situ discharges (Fig. B1; see location in Fig. 01) show an
646 overall satisfactory fit. For the Ubangui River and the Congo River, where the in-situ time series
647 are long, KGE reached 0.89 and 0.87, respectively. Although less meaningful because of shorter
648 time periods, the evaluation at Sangha and Ilebo also showed good agreement. Simulated
649 discharges indicate that MGB was able to successfully route the water along the basin. The
650 bimodality at Brazzaville is quite well represented, although there seems to be an issue regarding
651 the recession between the high flow peak (around December) and the second mode peak (around
652 March). This may be due to a lack of bimodality in the Kasai River simulated discharges, which
653 does not appear in the quality indicators due to the short length of Ilebo time series. At Brazzaville,
654 the mean annual discharge for the study period is $38,284 \text{ m}^3 \text{ s}^{-1}$, which is consistent with the 13
655 values provided in Laraque et al. [2013] and Moukandi et al. [this issue] for different studies and
656 periods.

657 For the four in-situ gauges shown above, the model performed slightly better than the GW-
658 PITMAN model presented in Tshimanga and Hughes [2014]. This result must be balanced by the
659 fact that the simulated period was much smaller in our study, and also that the analysis was made
660 in a monthly basis by Tshimanga and Hughes [2014]. It also performed better than the GeoSFM
661 model used by Munzimi et al. [2019]. ENS and KGE values are summarized in Table B1.

662 At Mbata (Lobaye River), the simulated discharges also compared well to the observed ones (Fig.
663 B2). This assertion is important because unlike the other four gages, the drainage area at Mbata is
664 low (around 180 km^2). Consequently, runoff generation mechanism at this part is much more
665 important than for large drained areas, where several processes such as flow propagation take more
666 importance.

667 Reaching such a good fit at Brazzaville while ensuring no over-parameterization was only possible
668 thanks to the virtual discharge time series that were added as calibration data (see Fig. 01). Fig. B3
669 provides the comparison of simulated and *virtual* discharges.

670 Once again, a good fit was achieved after calibration at all these locations, although KGE and ENS
671 values were slightly lower than those obtained for gaged discharges. At Kabalo (Lualaba River),
672 the peak discharge occurs slightly earlier than the observed one, which may be due to an
673 underestimation of the water residence time in the Upemba swamps. The discrepancies observed
674 between the two time series at Basankusu appear to be more due to errors in the conversion of
675 WSE into discharge or in the WSE time series than simulation errors themselves.

676 For the other five locations, namely Ingende (Ruki River), Kabalo (Upper Lualaba River), Dima
677 (Kasai River), Tchepakipa (Alima River) and Bwembe (Lefini River), overall good behavior is
678 observed. Higher discrepancies are obtained at Ingende (Ruki River), which highlights the
679 difficulty to properly model rainfall-runoff processes in the Central Cuvette with absolutely no
680 gage data on the study period, neither for surface water nor for groundwater. However, the ENS
681 and KGE achieved at Basankusu and Ingende, together with the satisfactory agreement at

682 Brazzaville, let us confident on the consistency of the discharges simulated in the Ruki and
683 Lulonga sub-basins.

684 It is interesting to note that the model also performed relatively well for the sub-basins from the
685 Batekes regions (Alima, Lefini, Linkula), although it was only calibrated against *virtual* gages
686 because no in-situ measurement is available in such locations in the last decade. The Batekes
687 region is well known for its important underground water and strongly regular flows. Our
688 simulations provide a distributed point of view of the recent hydrology of this region. The
689 performance indicator for each gage are presented in Table B1.

690

Appendix C: MGB model validation

691

692 It has been shown that the *Congolaise Cuvette* and the *Batekes Plateau* have a remarkably
 693 distinct hydrological behavior despite of their geographic proximity [Laraque et al., 1998b]. This
 694 highlights the importance of assessing the seasonal variability of discharge, which can be
 695 expressed by the ratio between maximum and minimum monthly discharge, as follows:

$$696 \quad SeV = \frac{\max(\overline{Q_m})}{\min(\overline{Q_m})} \quad (C1)$$

697 where $\overline{Q_m}$ stands for the mean monthly discharge computed from MGB simulations.

698 According to Laraque et al. [1998b], the SeV in the Batekes Rivers should range between 1.1 and
 699 1.5, while the Central Cuvette Rivers should reach values higher than 2. The values of SeV found
 700 in rivers from these two formations are summarized in Table C1. There is a clear difference in SeV
 701 values between two regions with the limit being the Likouala aux Herbes River, which is the first
 702 river considered as part of the Cuvette. Those values indicate that the ranges of monthly discharges
 703 in this region are globally consistent with those presented by Laraque et al. [1998b] from extensive
 704 ground surveys. SeV values taken from Laraque et al. [1998b] on the [1947 – 1993] period are
 705 also presented.

706 Fig. C1 provides an analysis on the contribution of each zone to the total flow at Brazzaville in the
 707 four trimesters of a year. It is evidenced that the Cuvette Centrale has an almost constant
 708 contribution (from 20% to 25% of the total flow). During the 1st and 2nd trimesters, the Northern
 709 Hemisphere Rivers (Ubangui and Sangha, mainly) contribute less than 6 and 9%, respectively.
 710 Their contribution reach almost 25% in the last trimester, when the Congo is reaching its peak
 711 flow. These results are similar to those from Bricquet [1993], however the contribution of the
 712 Cuvette was more variable in their study.

713 We also assessed the seasons for which the flow peak and minimum discharge are most likely to
 714 occur (Fig. C2). For visualization purposes, only reaches with topological order (see description
 715 in Collischonn et al. [2007] and Paiva et al. [2013]) higher than six were selected. The precipitation
 716 and hydrological regimes as described for instance by Bricquet [1993] and Alsdorf et al. [2016]
 717 and evidenced by Munzimi et al. [2019] were properly identified. This shows the consistency of
 718 the rainfall-runoff transformation process and also of the routing method, as the peaks and low
 719 flows seem to be adequately propagated.

720 **References**

- 721 Allen and Pavelsky (2018). Global Extent of Rivers and Streams. *Science*.
722 <https://doi.org/10.1126/science.aat0636>
- 723 Alsdorf, D., E. Beighley, A. Laraque, H. Lee, R. Tshimanga, F. O'Loughlin, G. Mahé, B. Dinga,
724 G. Moukandi, and R. G. M. Spencer (2016). Opportunities for hydrologic research in the Congo
725 Basin, *Rev. Geophys.*, 54, 378–409, doi:10.1002/2016RG000517.
- 726 Aloysius, N. and Saiers, J. (2017). Simulated hydrologic response to projected changes in
727 precipitation and temperature in the Congo River basin. *Hydrol. Earth Syst. Sci.*, 21, 4115–4130,
728 <https://doi.org/10.5194/hess-21-4115-2017>.
- 729 Andreadis, K. M., Schumann, G. J. P., & Pavelsky, T. (2013). A simple global river bankfull width
730 and depth database. *Water Resources Research*, 49(10), 7164-7168.
- 731 Andriambelason, J. A., Paris, A., Calmant, S., Rakotondraompiana, S. (accepted). Re-initiating
732 depth-discharge monitoring of small-sized ungaged watersheds by combining remote sensing and
733 hydrologic modelling: a case study in Madagascar. *Hydrological Sciences Journal*, in press.
- 734 Becker, M., Da Silva, J.S., Calmant, S., Robinet, V., Linguet, L., Seyler, F. (2014). Water Level
735 Fluctuations in the Congo Basin Derived from ENVISAT Satellite Altimetry. *Remote Sens.* 2014,
736 6, 9340-9358.
- 737 Becker, M.H., Papa, F.B., Frappart, F., Alsdorf, D., Calmant, S., Da, J., Silva, Prigent, C., &
738 Seyler, F. (2018). Satellite-based estimates of surface water dynamics in the Congo River Basin.
- 739 Beighley, R. E., Ray, R. L., He, Y., Lee, H., Schaller, L., Andreadis, K. M., Durand, M., Alsdorf,
740 D. E. and Shum, C. K. (2011). Comparing satellite derived precipitation datasets using the
741 Hillslope River Routing (HRR) model in the Congo River Basin. *Hydrol. Process.*, 25: 3216–3229.
742 doi:10.1002/hyp.8045.
- 743 Youssoufa Bele, M., Jean Sonwa, D., & Tiani, A. M. (2013). Supporting local adaptive capacity
744 to climate change in the Congo basin forest of Cameroon: A participatory action research
745 approach. *International Journal of Climate Change Strategies and Management*, 5(2), 181-197.
- 746 Bergonzini L., Williamson D., Albergel J. (2015). L'hydrologie et la limnologie autour du lac
747 Tanganyika. In : Cazenave-Piarrot A. (coord.), Ndayirukiye S. (coord.), Valton Catherine (coord.),
748 Gaudemar J.P. de (pref.), Moatti Jean-Paul (pref.). *Atlas des pays du Nord-Tanganyika*. Marseille
749 : IRD, 24-27. ISBN 978-2-7099-2152-7
- 750 Biancamaria, S., Hossain, F., & Lettenmaier, D. P. (2011). Forecasting transboundary river water
751 elevations from space. *Geophysical Research Letters*, 38(11).
- 752 Biancamaria, S., Lettenmaier, D. P., & Pavelsky, T. M. (2016). The SWOT Mission and Its
753 Capabilities for Land Hydrology. *Surveys in Geophysics*. [https://doi.org/10.1007/s10712-015-](https://doi.org/10.1007/s10712-015-9346-y)
754 [9346-y](https://doi.org/10.1007/s10712-015-9346-y)
- 755 Bogning, S., Frappart, F., Paris, A., Blarel, F., Niño, F., Picart, S. S., & Bricquet, J. P. (2020).
756 Hydro-climatology study of the Ogooué River basin using hydrological modeling and satellite
757 altimetry. *Advances in Space Research*. Boko, H. (2019),
758 [https://observers.france24.com/fr/20191220-rd-congo-plusieurs-quartiers-kisangani-inondes-](https://observers.france24.com/fr/20191220-rd-congo-plusieurs-quartiers-kisangani-inondes-apres-montee-eaux-fleuve)
759 [apres-montee-eaux-fleuve](https://observers.france24.com/fr/20191220-rd-congo-plusieurs-quartiers-kisangani-inondes-apres-montee-eaux-fleuve).

- 760 Bricquet, J. P. (1995). Les écoulements du Congo à Brazzaville et la spatialisation des apports.
761 Olivry, JC and Boulègue, J., Inst. Fr. de Rech. Sci. pour le Dev. en Coop.(ORSTOM), Paris, 27-
762 38.
- 763 BRLi. (2016), Développement et mise en place de l’outil de modélisation et d’allocation des
764 ressources en eau du Bassin du Congo : Rapport technique de construction et de calage du modèle,
765 CICOS, Kinshasa, RDC.
- 766 Bultot, F. (1971). Atlas Climatique du Bassin Congolais Publications de L’Institut National pour
767 L’Etude Agronomique du Congo (I.N.E.A.C.). Deuxieme Partie, Les Composantes du Bilan d’Eau.
- 768 Bwangoy, J. R. B., Hansen, M. C., Roy, D. P., De Grandi, G., & Justice, C. O. (2010). Wetland
769 mapping in the Congo Basin using optical and radar remotely sensed data and derived
770 topographical indices. *Remote Sensing of Environment*, 114(1), 73-86.
- 771 Calmant, S., and F. Seyler (2006). Continental surface water from satellite altimetry. *C. R. Geosci.*,
772 338(14–15), 1113–1122, doi:10.1029/2001JD000609.
- 773 Calmant, S., F. Seyler, and J. F. Cretaux (2008). Monitoring continental surface waters by satellite
774 altimetry. *Surv. Geophys.*, 29, 247–269.
- 775 Calmant, S., J. Santos da Silva, D. Medeiros Moreira, F. Seyler, C. K. Shum, J.-F. Crétaux, and G.
776 Gabalda (2012). Detection of ENVISAT RA2/ICE-1 retracked Radar Altimetry Bias over the
777 Amazon Basin Rivers using GPS. *Adv. Space Res.*, 51(8), 1551–1564,
778 doi:10.1016/j.asr.2012.07.033.
- 779 Carr, A. B., Trigg, M. A., Tshimanga, R.M., Borman, D. J., and Smith, M. W. (2019). Greater
780 water surface variability revealed by new Congo Riverfield data: Implications for satellite altimetry
781 measurements of large rivers. *Geophysical Research Letters*, 46, 8093–46,8101.
782 <https://doi.org/10.1029/2019GL083720>.
- 783 Charlier, J. (1955). Études hydrographiques dans le bassin du Lualaba.
- 784 Chen, C., Desai, S., Picot, N., Fu, L.-L., Morrow, R., Pavelsky, T., Cretaux, J.-F. (2018). SWOT
785 Calibration / Validation Plan, available at [https://swot.jpl.nasa.gov/docs/D-](https://swot.jpl.nasa.gov/docs/D-75724_SWOT_Cal_Val_Plan_Initial_20180129u.pdf)
786 [75724_SWOT_Cal_Val_Plan_Initial_20180129u.pdf](https://swot.jpl.nasa.gov/docs/D-75724_SWOT_Cal_Val_Plan_Initial_20180129u.pdf).
- 787 Chishugi, J. B., & Alemaw, B. F. (2009). The hydrology of the Congo River Basin: A GIS-based
788 hydrological water balance model. In *World Environmental and Water Resources Congress 2009:*
789 *Great Rivers* (pp. 1-16).
- 790 Collischonn, W., Allasia, D. G., Silva, B. C., Tucci, C. E. M. (2007). The MGB-IPH model for
791 large-scale rainfall-runoff modelling. *Hydrological Sciences Journal*, v. 52, p. 878-895, 2007.
- 792 Crétaux, J. F., & Birkett, C. (2006). Lake studies from satellite radar altimetry. *Comptes Rendus*
793 *Geoscience*, 338(14-15), 1098-1112.
- 794 Crétaux, J. F., Abarca-del-Río, R., Berge-Nguyen, M., Arsen, A., Drolon, V., Clos, G., &
795 Maisongrande, P. (2016). Lake volume monitoring from space. *Surveys in Geophysics*, 37(2), 269-
796 305.
- 797 CruHM Newsletter Edition 2, January 2018
- 798 Dargie, G. C., S. L. Lewis, I. T. Lawson, E. T. Mitchard, S. E. Page, Y. E. Bocko, and S. A. Ifo
799 (2017). Age, extent and carbon storage of the central Congo Basin peatland complex, *Nature*.

- 800 Devroey, E.-J. (1955). *Annuaire hydrologique du Congo belge et du Ruandi-Urundi*(1954). T.III,1
801 Devroey, E.-J. (1956). *Annuaire hydrologique du Congo belge et du Ruandi-Urundi*(1955). T.V,2
- 802 Di Baldassarre, G., & Montanari, A. (2009). Uncertainty in river discharge observations: A
803 quantitative analysis. *Hydrology and Earth System Sciences*, 13(6), 913–921.
804 <https://doi.org/10.5194/hess-13-913-2009>
- 805 Domeneghetti, A., Tarpanelli, A., Brocca, L., Barbetta, S., Moramarco, T., Castellarin, A., &
806 Brath, A. (2014). The use of remote sensing-derived water surface data for hydraulic model
807 calibration. *Remote sensing of environment*, 149, 130-141.
- 808 Emery, C. M., Paris, A., Biancamaria, S., Boone, A., Calmant, S., Garambois, P. A., & Da Silva,
809 J. S. (2017). Large scale hydrological model river storage and discharge correction using satellite
810 altimetry-based discharge product. *Hydrology and Earth System Sciences Discussions*, 22, 2135-
811 2162.
- 812 Eyers, R.; Obowu, C.; Lasisi, B. (2013). Niger Delta Flooding: Monitoring, Forecasting &
813 Emergency Response Support from SPDC. In *Proceedings of the FIG Working Week*,
814 *Environment and Sustainability*, Abuja, Nigeria, 6–10 May 2013.
- 815 Fleischmann, A., Siqueira, V., Paris, A., Collischonn, W., Paiva, R., Pontes, P., ... and Calmant,
816 S. (2018). Modelling hydrologic and hydrodynamic processes in basins with large semi-arid
817 wetlands. *Journal of hydrology*, 561, 943-959.
- 818 Fluet-Chouinard, E., Lehner, B., Rebelo, L. M., Papa, F., & Hamilton, S. K. (2015). Development
819 of a global inundation map at high spatial resolution from topographic downscaling of coarse-scale
820 remote sensing data. *Remote Sensing of Environment*, 158, 348-361.
- 821 Garambois, P. A., Calmant, S., Roux, H., Paris, A., Monnier, J., Finaud-Guyot, P., ... & Santos da
822 Silva, J. (2017). Hydraulic visibility: Using satellite altimetry to parameterize a hydraulic model
823 of an ungauged reach of a braided river. *Hydrological processes*, 31(4), 756-767.
- 824 Getirana, A. C., Bonnet, M. P., Calmant, S., Roux, E., Rotunno Filho, O. C., & Mansur, W. J.
825 (2009). Hydrological monitoring of poorly gauged basins based on rainfall–runoff modeling and
826 spatial altimetry. *Journal of hydrology*, 379(3-4), 205-219.
- 827 Getirana, A., Jung, H. C., Van Den Hoek, J., & Ndehedehe, C. E. (2020). Hydropower dam
828 operation strongly controls Lake Victoria's freshwater storage variability. *Science of The Total*
829 *Environment*, 138343.
- 830 Gleason, C. J., & Smith, L. C. (2014). Toward global mapping of river discharge using satellite
831 images and at-many-stations hydraulic geometry. *Proceedings of the National Academy of*
832 *Sciences*, 111(13), 4788-4791.
- 833 Gleason, C. J., & Wang, J. (2015). Theoretical basis for at-many-stations hydraulic geometry.
834 *Geophysical Research Letters*, 42(17), 7107-7114.
- 835 Gosset M, Alcoba M, Roca R, Cloché S, Urbani G. (2018). Evaluation of TAPEER daily estimates
836 and other GPM-era products against dense gauge networks in West Africa, analysing ground
837 reference uncertainty. *QJRMeteorolSoc*; 144 (Suppl.1): 255–269. <https://doi.org/10.1002/qj.3335>
- 838 GRDC (2019), https://www.bafg.de/GRDC/EN/02_srvcs/21_tmsrs/riverdischarge_node.html.

- 839 Gupta, H. V., Kling, H., Yilmaz, K. K., & Martinez, G. F. (2009). Decomposition of the mean
840 squared error and NSE performance criteria: Implications for improving hydrological modelling.
841 *Journal of hydrology*, 377(1-2), 80-91.
- 842 Hastenrath, S. (1985), *Climate and circulation of the tropics*, Springer Netherlands, Dordrecht.
- 843 Hoch, J. M., Haag, A. V., Dam, A. V., Winsemius, H. C., van Beek, L. P., & Bierkens, M. F.
844 (2017). Assessing the impact of hydrodynamics on large-scale flood wave propagation—a case
845 study for the Amazon Basin. *Hydrology and Earth System Sciences*, 21(1), 117-132.
- 846 Hughes and Hughes, (1987). *a directory of African wetlands*.
- 847 Hughes, D. A., Tshimanga, R. M., Tirivarombo, S. And Tanner, J. (2013). Simulating wetland
848 impacts on stream flow in southern Africa using a monthly hydrological model. *Hydrol. Processes*,
849 28 (4), 1775-1786, doi: 10.1002/hyp.9725.
- 850 Jung, H.C., Getirana, A., Policelli, F., McNally, A., Arsenault, K.R., Kumar, S., Tadesse, T.,
851 Peters-Lidard, C.D. (2017). Upper Blue Nile Basin Water Budget from a Multi-Model
852 Perspective, *Journal of Hydrology*, doi: <https://doi.org/10.1016/j.jhydrol.2017.10.040>.
- 853 Ekeu-wei, I.T. and Blackburn, G.A. (2018). Applications of Open-Access Remotely Sensed Data
854 for Flood Modelling and Mapping in Developing Regions. *Hydrology* 2018, 5, 39.
- 855 Kim, D., Lee, H., Laraque, A., Tshimanga, R. M., Yuan, T., Jung, H. C., ... & Chang, C. H. (2017).
856 Mapping spatio-temporal water level variations over the central Congo River using PALSAR
857 ScanSAR and Envisat altimetry data. *International Journal of Remote Sensing*, 38(23), 7021-7040.
- 858 Kim, D., Yu, H., Lee, H., Beighley, E., Durand, M., Alsdorf, D. E., and Hwang, E. (2019).
859 Ensemble learning regression for estimating river discharges using satellite altimetry data: Central
860 Congo River as a Test-bed. *Remote sensing of environment*, 221, 741-755.
- 861 Knoben, W. J. M., Freer, J. E., and Woods, R. A.: Technical note: Inherent benchmark or not?
862 Comparing Nash–Sutcliffe and Kling–Gupta efficiency scores, *Hydrol. Earth Syst. Sci.*, 23, 4323–
863 4331, <https://doi.org/10.5194/hess-23-4323-2019>, 2019.
- 864 Kolding, J., Ticheler, H., & Chanda, B. (2008). THE BANGWEULU SWAMPS – A BALANCED
865 SMALL-SCALE MULTISPECIES FISHERY.
- 866 Laraque A., Olivry J. C. (1998). Deux systèmes hydrologiques mitoyens mais opposés du bassin
867 du Congo-Zaïre: la cuvette congolaise et les plateaux tékés. In : Demarée G. (ed.), Alexandre J.
868 (ed.), De Dapper M. (ed.) *Tropical climatology, meteorology and hydrology: in memoriam Franz*
869 *Bultot (1924-1995)*. IRM ; ARSOM, 593-606. *Tropical Climatology, Meteorology and*
870 *Hydrology: International Conference, Bruxelles (BEL), 1996/05/22-24*.
- 871 Laraque, A., & Olivry, J. C. (1996). Evolution de l'hydrologie du Congo-Zaïre et de ses affluents
872 rive droite et dynamique des transports solides et dissous. *IAHS PUBLICATION*, 271-288.
- 873 Laraque, A., B. Pouyaud, R. Rocchia, R. Robin, I. Chaffaut, J.-M. Moutsambote, B. Maziezoula,
874 C. Censier, Y. Albouy, H. Elenga, H. Etcheber, M. Delaune, F. Sondag, F. Gasse (1998a). Origin
875 and function of a closed depression in equatorial humid zones: the lake Tele in north Congo.
876 *Journal of Hydrology* 207, 236–253.

- 877 Laraque, A., Mietton, M., Olivry, J., & Pandic, A. (1998b). Influence des couvertures lithologiques
878 et végétales sur les régimes et la qualité des eaux des affluents congolais du fleuve Congo. *Revue*
879 *des sciences de l'eau/Journal of Water Science*, 11(2), 209-224.
- 880 Laraque, A., J.P. Bricquet, A. Pandi, and J.C. Olivry (2009). A review of material transport by the
881 Congo river and its tributaries. *Hydrological Processes* 23, 3216-3224.
- 882 Laraque, A., Bellanger, M., Adèle, G., Guebanda, S., Gulemvuga, G., Pandi, A., ... & Yambele,
883 A. (2013). Recent evolution of the Congo, Ubangui and Sangha River flows. *Acad. R. Sci. Bel.,*
884 *Geo-Eco-Trop*, 37(1), 93-100.
- 885 Lee, H., Yuan, T., Jung, H. C., & Beighley, E. (2015). Mapping wetland water depths over the
886 central Congo Basin using PALSAR ScanSAR, Envisat altimetry, and MODIS VCF data.
887 *Remote Sensing of Environment*, 159, 70–79. <https://doi.org/10.1016/j.rse.2014.11.030>
- 888 Leon, J. G., Calmant, S., Seyler, F., Bonnet, M. P., Cauhopé, M., Frappart, F., ... & Fraizy, P.
889 (2006). Rating curves and estimation of average water depth at the upper Negro River based on
890 satellite altimeter data and modeled discharges. *Journal of hydrology*, 328(3-4), 481-496.
- 891 Logah, F. Y., Amisigo, A. B., Obuobie, E., & Kankam-Yeboah, K. (2017). Floodplain
892 hydrodynamic modelling of the Lower Volta River in Ghana. *Journal of Hydrology: Regional*
893 *Studies*, 14, 1-9. Magis, N. (1962). Étude limnologique des lacs artificiels de la Lufira et du Lualaba
894 (Haut Katanga) I. Le régime hydraulique, les variations saisonnières de la température. *Int. Revue*
895 *ges. Hydrobiol. Hydrogr.*, 47: 33–84. doi:10.1002/iroh.19620470104
- 896 Mahé, G., and J.-C. Olivry (1995). Variations des précipitations et des écoulements en Afrique de
897 l'Ouest et centrale de 1951 à 1989. *Science et changements planétaires/Sécheresse*, 6(1), 109–117.
- 898 Moukandi G.D., A. Laraque, J-E. Paturel, G. Gulemvuga, G. Mahé, R. Tshimanga Muamba.
899 (accepted). A new look at hydrology in the Congo Basin, based on the study of multi-decadal
900 chronicles. In *Congo Basin Hydrology, Climate, and Biogeochemistry: A Foundation for the*
901 *Future*, Alsdorf, D., Tshimanga Muamba, R. Moukandi N'kaya, G.D., eds, AGU, John Wiley &
902 Sons Inc.
- 903 Munzimi, Y. A., Hansen, M. and Kwabena O. Asante, K.-O. (2019). Estimating daily streamflow
904 in the Congo Basin using satellite-derived data and a semi-distributed hydrological model.
905 *Hydrological Sciences Journal*, 64:12, 1472-1487, DOI: 10.1080/02626667.2019.1647342.
- 906 Ndehedehe, C. E., Awange, J. L., Kuhn, M., Agutu, N. O., & Fukuda, Y. (2017). Analysis of
907 hydrological variability over the Volta river basin using in-situ data and satellite observations.
908 *Journal of Hydrology: Regional Studies*, 12, 88-110.
- 909 New, M., Lister, D., Hulme, M., & Makin, I. (2002). A high-resolution data set of surface climate
910 over global land areas. *Climate research*, 21(1), 1-25.
- 911 Nguimalet, C. R. and Orange, D. (2013). Dynamique hydrologique récente de l'Ubangui à Bangui
912 (Centrafrique) : impacts anthropiques ou climatiques ?" *Geo-Eco-Trop*, 37, Tome 1, pp. 101-112.
- 913 Nguimalet, C. R. (2017). Changements enregistrés sur les extrêmes hydrologiques de l'Ubangui à
914 Bangui (République centrafricaine) : analyse des tendances. *Rev. Sci. Eau*, 30 (3), 183–196.
- 915 Nguimalet, C. R., & Orange, D. (2019). Caractérisation de la baisse hydrologique actuelle de la
916 rivière Ubangui à Bangui, République Centrafricaine. *La Houille Blanche*, (1), 78-84.

- 917 O'Loughlin, F., Trigg, M. A., Schumann, G. P., & Bates, P. D. (2013). Hydraulic characterization
918 of the middle reach of the Congo River. *Water Resources Research*, 49(8), 5059-5070.
- 919 O'Loughlin, F., J. Neal, G.J.P. Schumann, E. Beighley, P.D. Bates. (2020). A LISFLOOD-FP
920 hydraulic model of the middle reach of the Congo, *Journal of Hydrology*, Volume 580, 2020,
921 124203, ISSN 0022-1694, <https://doi.org/10.1016/j.jhydrol.2019.124203>.
- 922 Olivry, J. C., Bricquet, J. P., & Thiébaux, J. P. (1989). Bilan annuel et variations saisonnières des
923 flux particuliers du Congo à Brazzaville et de l'Oubangui à Bangui. *La Houille Blanche*, (3-4),
924 311-316.
- 925 Paiva, R. C. D., Collischonn, W., Buarque, D. C. (2013). Validation of a full hydrodynamic model
926 for large scale hydrologic modelling in the Amazon. *Hydrological Processes*, 27, p. 333–346. DOI:
927 10.1002/hyp.8425, 2013.
- 928 Paiva, R. C. D., Collischonn, W., Bonnet, M. P., De Goncalves, L. G. G., Calmant, S., Getirana,
929 A., & Santos da Silva, J. (2013a). Assimilating in situ and radar altimetry data into a large-scale
930 hydrologic-hydrodynamic model for streamflow forecast in the Amazon. *Hydrology and Earth
931 System Sciences*, 17(7), 2929-2946.
- 932 Papa, F., Durand, F., Rossow, W. B., Rahman, A., & Bala, S. K. (2010). Satellite altimeter-derived
933 monthly discharge of the Ganga-Brahmaputra River and its seasonal to interannual variations from
934 1993 to 2008. *Journal of Geophysical Research: Oceans*, 115(C12).
- 935 Paris, A., Dias de Paiva, R., Santos da Silva, J., Medeiros Moreira, D., Calmant, S., Garambois, P.
936 A., Collischonn W., Bonnet, M. P. and Seyler, F. (2016). Stage-discharge rating curves based on
937 satellite altimetry and modeled discharge in the Amazon basin. *Water Resources Research*, 52(5),
938 3787-3814.
- 939 Paris, A. (2015). Utilisation conjointe de données d'altimétrie satellitaire et de modélisation pour
940 le calcul des débits distribués dans le bassin amazonien (Doctoral dissertation, Université de
941 Toulouse, Université Toulouse III - Paul Sabatier).
- 942 Pekel, J. F., Cottam, A., Gorelick, N., & Belward, A. S. (2016). High-resolution mapping of global
943 surface water and its long-term changes. *Nature*, 540(7633), 418-422.
- 944 Poméon, T., Dieckkrüger, B., & Kumar, R. (2018). Computationally efficient multivariate
945 calibration and validation of a grid-based hydrologic model in sparsely gauged West African river
946 basins. *Water*, 10(10), 1418.
- 947 Pontes, P. R. M., Fan, F. M., Fleischmann, A. S., de Paiva, R. C. D., Buarque, D. C., Siqueira, V.
948 A., ... & Collischonn, W. (2017). MGB-IPH model for hydrological and hydraulic simulation of
949 large floodplain river systems coupled with open source GIS. *Environmental modelling &
950 software*, 94, 1-20.
- 951 Revel, M., Ikeshima, D., Yamazaki, D., & Kanae, S. (2019). A Physically Based Empirical
952 Localization Method for Assimilating Synthetic SWOT Observations of a Continental-Scale
953 River: A Case Study in the Congo Basin. *Water*, 11(4), 829.
- 954 Roca, R., Taburet, N., Lorient, E., Chambon, P., Alcoba, M., Brogniez, H., ... & Guilloteau, C.
955 (2018). Quantifying the contribution of the Megha-Tropiques mission to the estimation of daily
956 accumulated rainfall in the Tropics. *Quarterly Journal of the Royal Meteorological Society*, 144,
957 49-63.

- 958 Rodier, J.-A. (1983). Aspects scientifiques et techniques de l'hydrologie des zones humides de
959 l'Afrique centrale. Proceedings of the Hamburg symposium. IAHS Publ no 140: 105-126, 1983.
- 960 Roux, E., Cauhope, M., Bonnet, M. P., Calmant, S., Vauchel, P., & Seyler, F. (2008). Daily water
961 stage estimated from satellite altimetric data for large river basin monitoring. *Hydrological
962 Sciences Journal*, 53(1), 81-99.
- 963 Samba, G., and D. Nganga (2012). Rainfall variability in Congo-Brazzaville: 1932–2007.
964 *International Journal of Climatology*, 32(6), 854–873.
- 965 Santos da Silva, J., S. Calmant, F. Seyler, O. C. Rotunno Filho, G. Cochonneau, and W. J. Mansur
966 (2010). Water levels in the Amazon basin derived from the ERS 2 and ENVISAT radar altimetry
967 missions. *Remote Sens. Environ.*, 114(10), 2160–2181.
- 968 Santos da Silva, J., S. Calmant, F. Seyler, H. Lee, and C. K. Shum (2012). Mapping of the Extreme
969 Stage variations using ENVISAT altimetry in the Amazon basin Rivers. *Int. Water Tech. J.*, 2(1),
970 14–25.
- 971 Schlosser, C.A., K. Strzepek, X. Gao, C. Fant, É. Blanc, S. Paltsev, H. Jacoby, J. Reilly and A.
972 Gueneau (2014). The future of global water stress: An integrated assessment. *Earth's Future*, 2(8):
973 341-361, doi:10.1002/2014EF000238.
- 974 Schröder, S., Springer, A., Kusche, J., Uebbing, B., Fenoglio-Marc, L., Diekkrüger, B., and
975 Poméon, T. (2019). Niger discharge from radar altimetry: bridging gaps between gauge and
976 altimetry time series. *Hydrol. Earth Syst. Sci.*, 23, 4113–4128, [https://doi.org/10.5194/hess-23-
977 4113-2019](https://doi.org/10.5194/hess-23-4113-2019).
- 978 Seyler, F., S. Calmant, J. Santos da Silva, D. Medeiros Moreira, F. Mercier, and C. K. Shum
979 (2013). From Topex/Poseidon to Jason-2/OSTM in the Amazon basin, *Adv. Space Res.*, 51(8),
980 1542–1550, doi:10.1016/j.asr.2012.11.002.
- 981 Siderius, C., Biemans, H., Kashaigili, J. J., & Conway, D. (2018). Going local: Evaluating and
982 regionalizing a global hydrological model's simulation of river flows in a medium-sized East
983 African basin. *Journal of Hydrology: Regional Studies*, 19, 349-364.
- 984 Siqueira, Vinícius Alencar, Fleischmann, Ayan, Jardim, Pedro Frediani, Fan, Fernando Mainardi,
985 & Collischonn, Walter. (2016). IPH-Hydro Tools: a GIS coupled tool for watershed topology
986 acquisition in an open-source environment. *RBRH*, 21(1), 274-287.
987 <https://dx.doi.org/10.21168/rbrh.v21n1.p274-287>.
- 988 Siqueira, V. A., Paiva, R. C. D. D., Fleischmann, A. S., Fan, F. M., Ruhoff, A. L., Pontes, P. R.
989 M., ... & Collischonn, W. (2018). Toward continental hydrologic–hydrodynamic modeling in
990 South America. *Hydrology and Earth System Sciences*. Göttingen: Copernicus. Vol. 22, n. 9 (set.
991 2018), p. 4815-4842.
- 992 Spencer, R. G., Hernes, P. J., Dinga, B., Wabakanghanzi, J. N., Drake, T. W., & Six, J. (2016).
993 Origins, seasonality, and fluxes of organic matter in the Congo River. *Global Biogeochemical
994 Cycles*, 30(7), 1105-1121.
- 995 Syed, T. H., J. S. Famiglietti, and D. P. Chambers (2009). GRACE based estimates of terrestrial
996 freshwater discharge from basin to continental scales. *J. Hydrometeorol.*, 10, 22–40,
997 doi:10.1175/2008JHM993.1.

- 998 Tarpanelli, A., Barbetta, S., Brocca, L., & Moramarco, T. (2013). River discharge estimation by
999 using altimetry data and simplified flood routing modeling. *Remote Sensing*, 5(9), 4145-4162.
- 1000 Tshimanga, R. M., and D. A. Hughes (2011). Climate change and impacts on the hydrology of the
1001 Congo Basin: The case of the northern sub-basins of the Ubangui and Sangha Rivers. *Phys. Chem.
1002 Earth*, 50-52, 72–83, doi:10.1016/j.pce.2011.07.045.
- 1003 Tshimanga, R. M., and D. A. Hughes (2014). Basin-scale performance of a semi-distributed
1004 rainfall-runoff model for hydrological predictions and water resources assessment of large rivers:
1005 The Congo River. *Water Resour. Res.*, 50, 1174–1188, doi:10.1002/2013WR014310.
- 1006 Voiland, A. (2019). https://www.nasa.gov/topics/earth/features/nox_lightning.html.
- 1007 Yamazaki, D., O'Loughlin, F., Trigg, M. A., Miller, Z. F., Pavelsky, T. M., & Bates, P. D. (2014).
1008 Development of the global width database for large rivers. *Water Resources Research*, 50(4),
1009 3467-3480.
- 1010 Yamazaki, D., Ikeshima, D., Tawatari, R., Yamaguchi, T., O'Loughlin, F., Neal, J. C., ... & Bates,
1011 P. D. (2017). A high-accuracy map of global terrain elevations. *Geophysical Research Letters*,
1012 44(11), 5844-5853.
- 1013 Yuan, T., Lee, H., & Jung, H. C. (2017). Congo floodplain hydraulics using PALSAR InSAR and
1014 Envisat altimetry data. *Remote Sensing of Hydrological Extremes* (pp. 65-81). Springer, Cham,
1015 65-81.
1016

1017 *Table 1: Rating curve coefficients at the Sentinel3-B VS (pass 541) obtained from the AMHG*
1018 *relationships and remote sensing datasets.*

<i>Width (m)</i>	<i>Slope (m/km)</i>	<i>Manning roughness</i>	<i>Coefficient a</i>	<i>Coefficient b</i>	<i>Coefficient Z0 (m)</i>
4000	0.047	0.035	695	1.864	352

1019

1020

1021 *Table B1: Quality indicators at each gage considered in this chapter. Drainage area is taken*
 1022 *from automatic discretization of the basin.*

Type	Name	River	A_d (10^3 km ²)	KGE	NSE
Gage (intl database)	Bangui	Ubangui	521	0.89	0.91
	Ouessou	Sangha	160	0.88	0.86
	Ilebo	Kasaï	247	0.81	0.77
	Brazzaville	Congo	3722	0.87	0.83
<i>Gage (this team)</i>	Mbata	Lobaye	32	0.93	0.87
Virtual gage (this study)	Kabalo	Lualaba	450	0.71	0.50
	Ntoken	Linkula	46	0.77	0.50
	Basankusu	Lulonga	71	0.61	0.64
	Yambuya	Aruwimi	107	0.75	0.57
	Ingende	Ruki	168	0.32	0.17
	Mulongo	Lualaba	157	0.87	0.86
	Lediba	Kasaï	892	0.91	0.89
	Tchepakipa	Alima	22	0.69	0.40
	Bwembe	Lefini	8	0.55	0.45
Kasenga	Luapula	160	0.69	0.39	

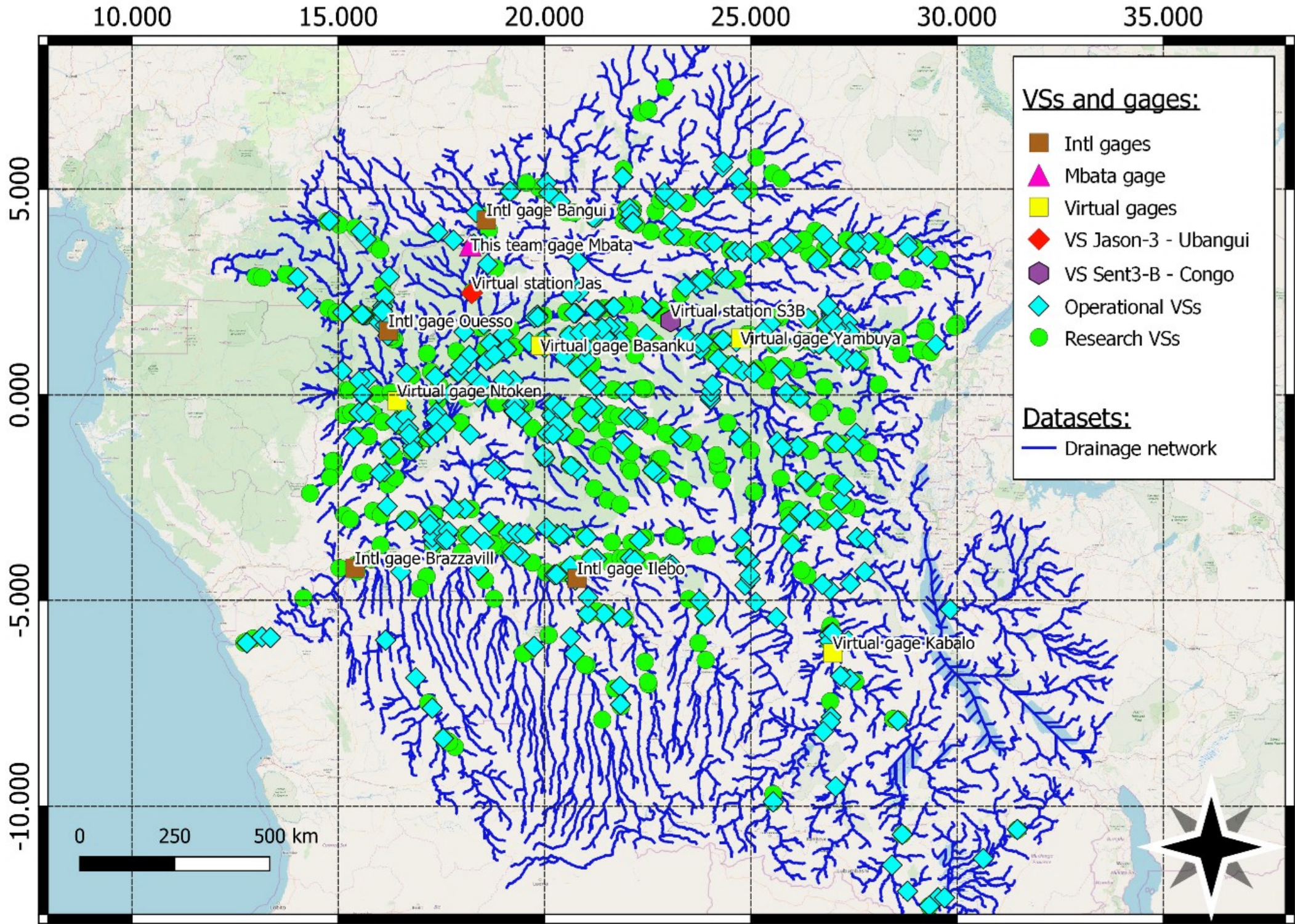
1023

1024

1025 *Table C1: SeV values for rivers located in the Bateke Plateau and the Congolaise Cuvette.*
 1026 *Values from MGB simulation and in-situ measurements.*

<i>Formation</i>	<i>River (station)</i>	<i>SeV (MGB)</i>	<i>SeV (in-situ)</i>
<i>Batekes</i>	Alima (Tchicapika)	1.33	1.28
	Lefini (Bwembé)	1.55	1.24
<i>Cuvette</i>	Likouala aux herbes (Botouali)	2.58	5.36
	Ndjiri (Pont RN2)	2.65	1.13
	Likouala Mossaka (Makoua)	2.69	3.34
	Kouyo (Owando)	2.11	2.14

1027



20.0

30.0

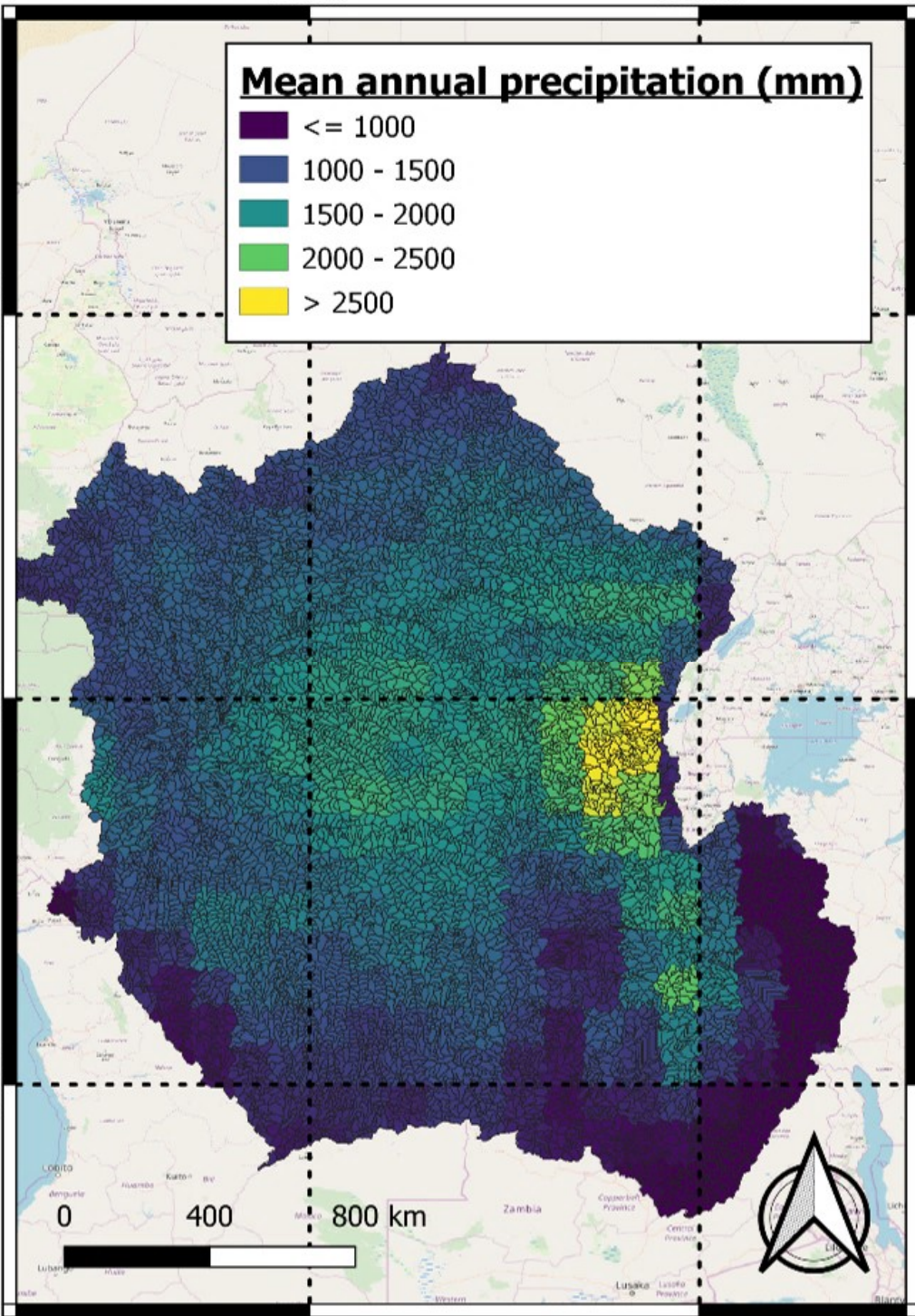
Mean annual precipitation (mm)

- <= 1000
- 1000 - 1500
- 1500 - 2000
- 2000 - 2500
- > 2500

10.0

0.0

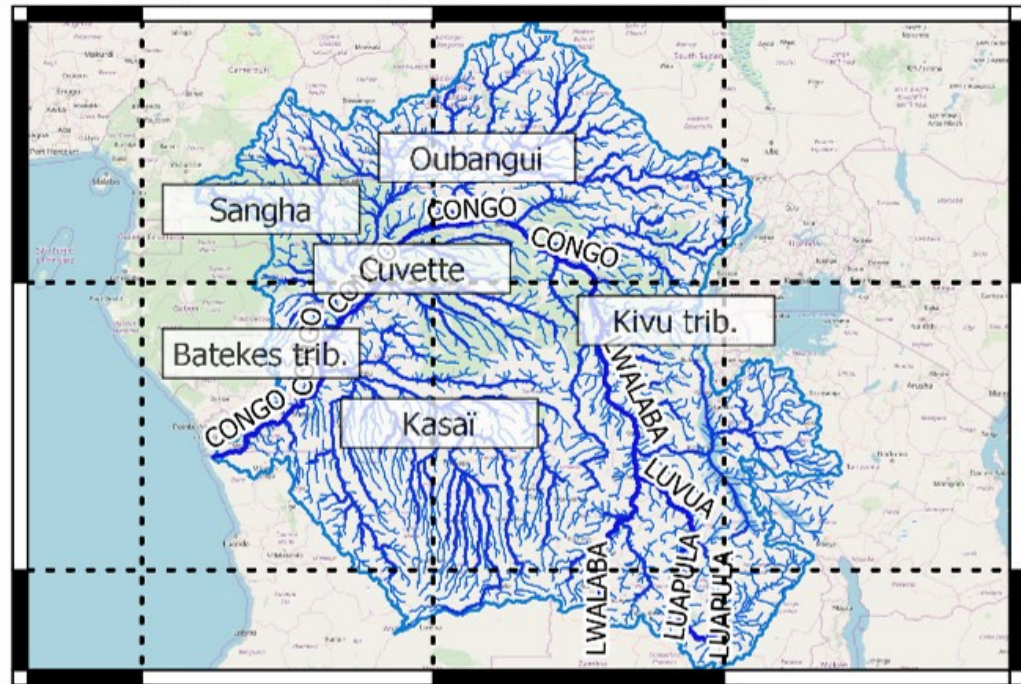
-10.0



10.0

20.0

30.0



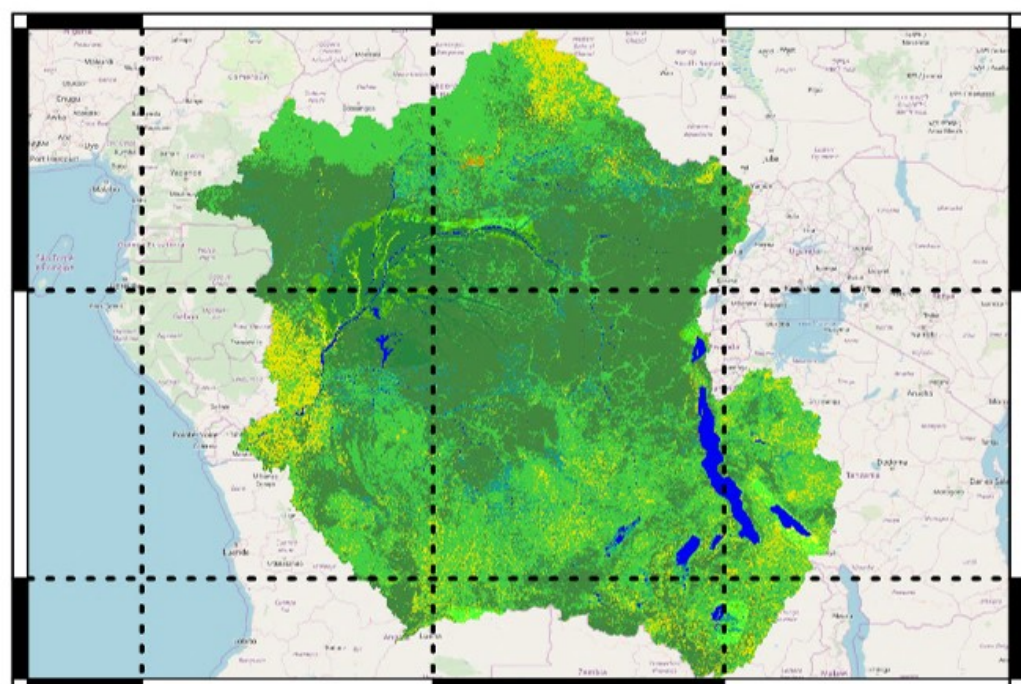
0.0

-10.0

10.0

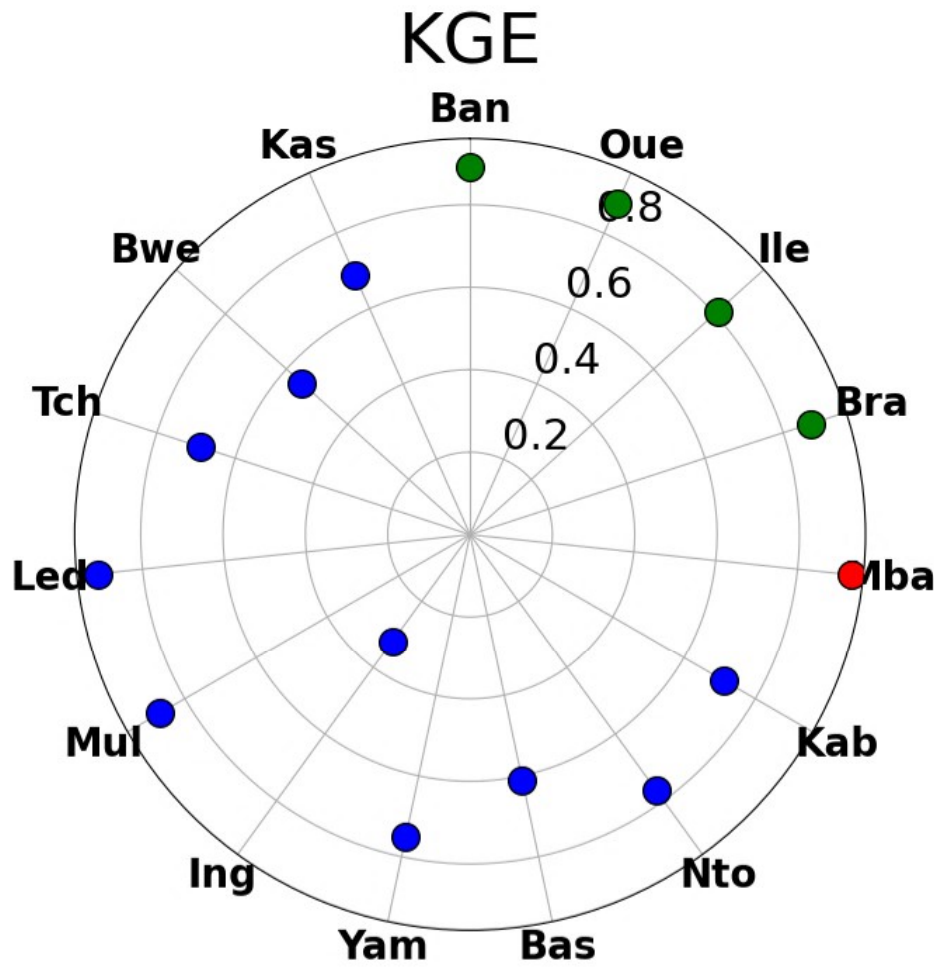
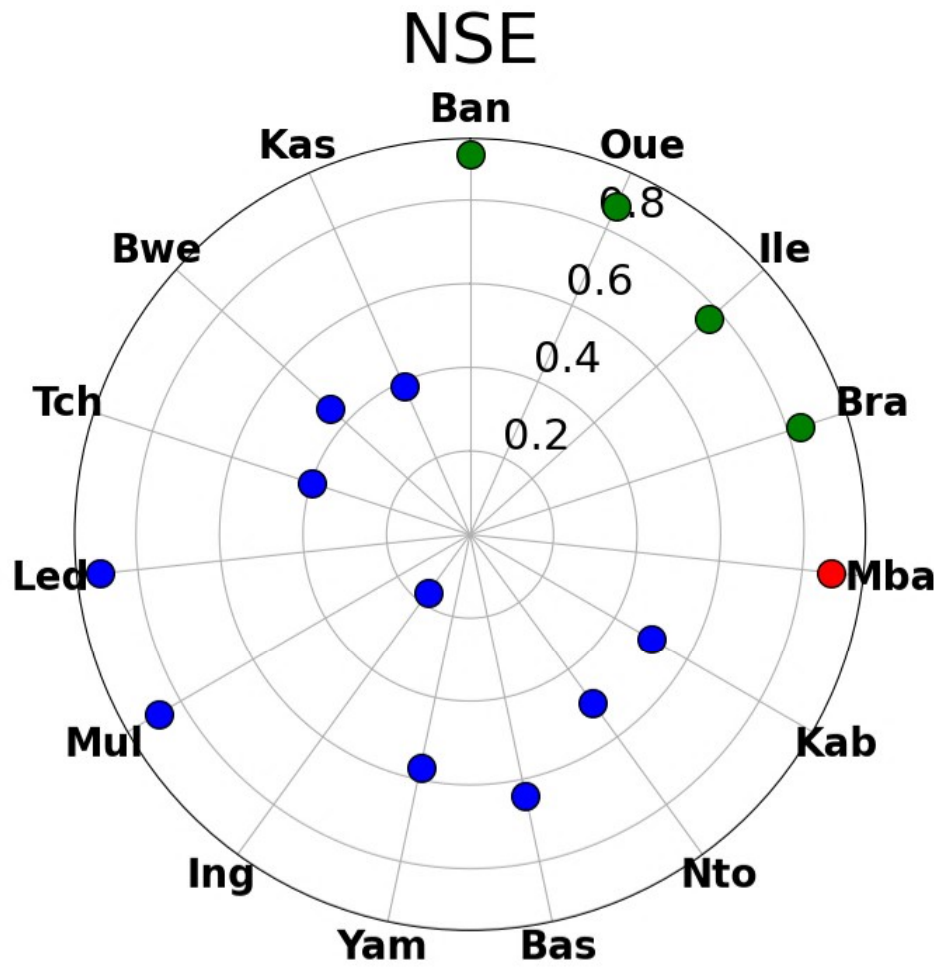
20.0

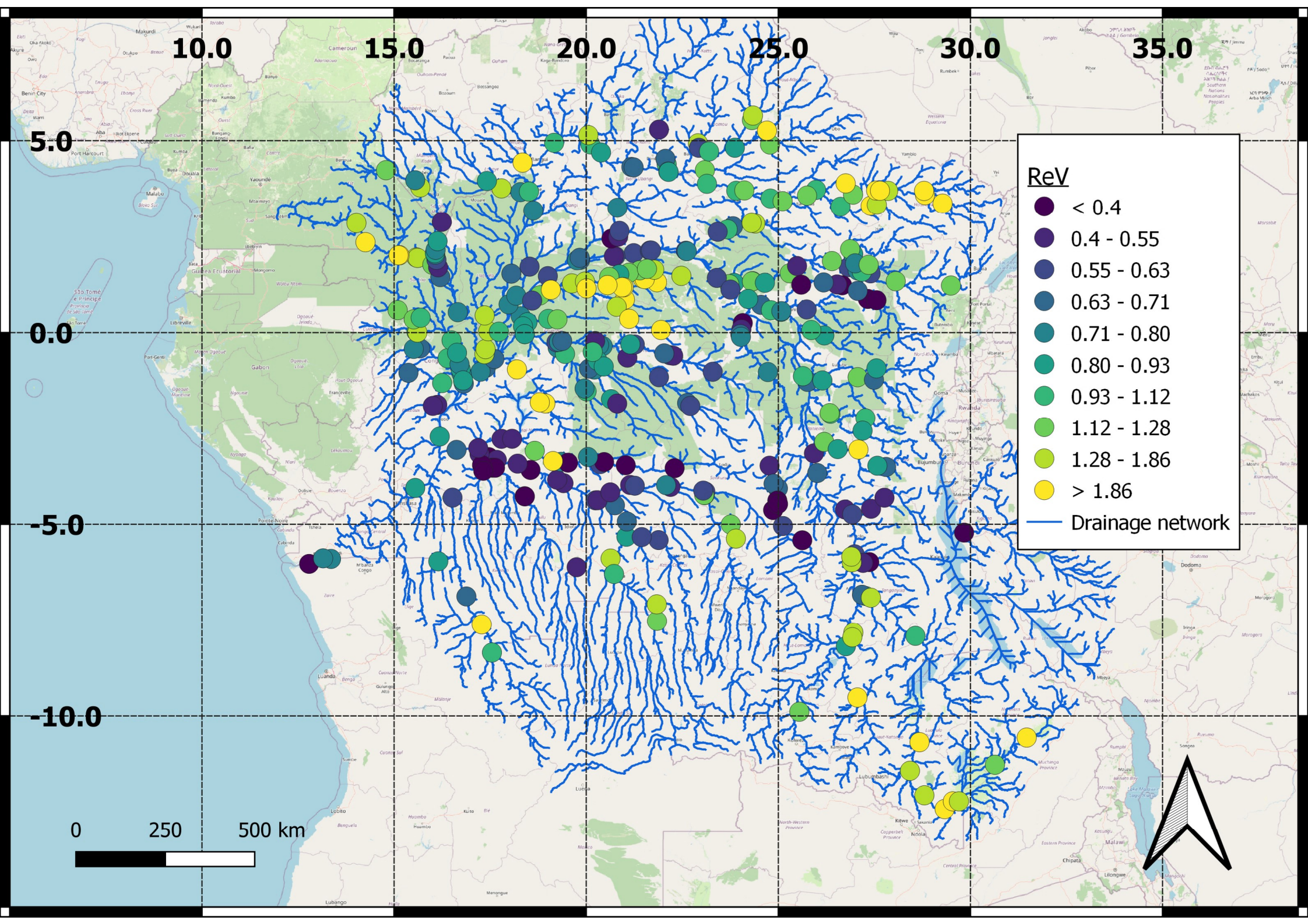
30.0

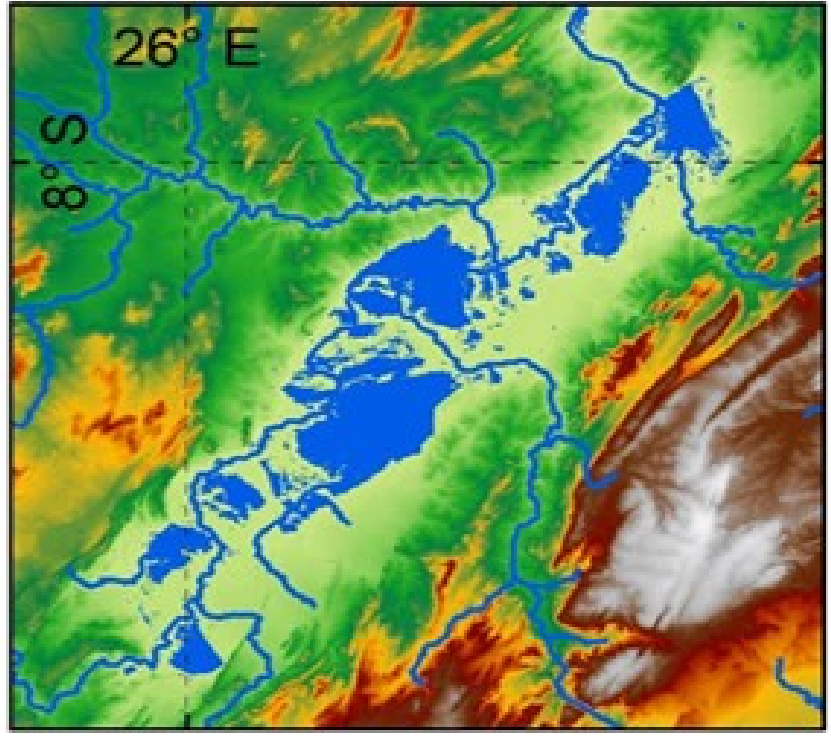
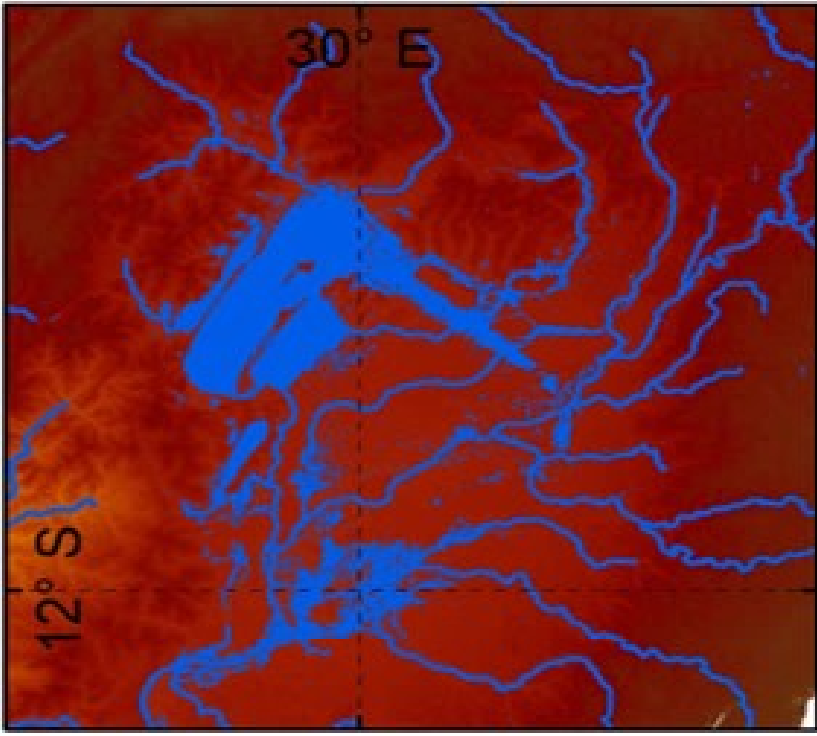
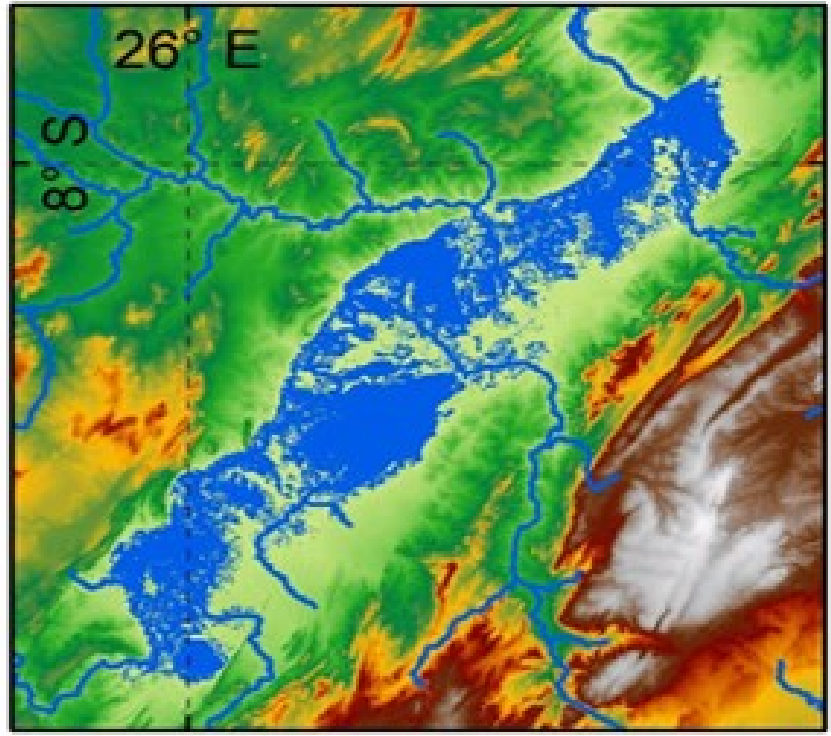
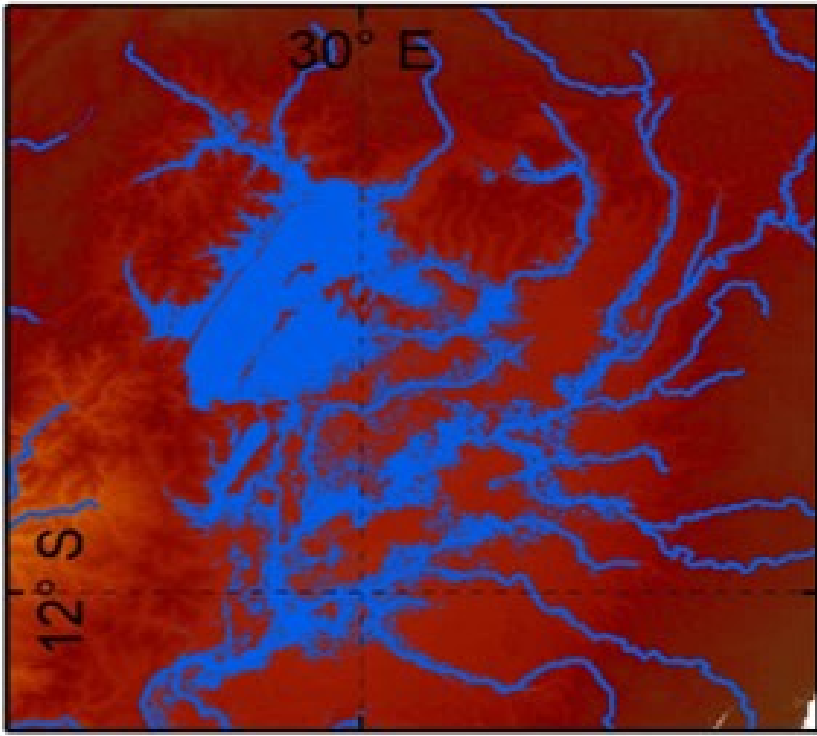


0.0

-10.0







16.000

18.000

20.000

16.000

18.000

20.000

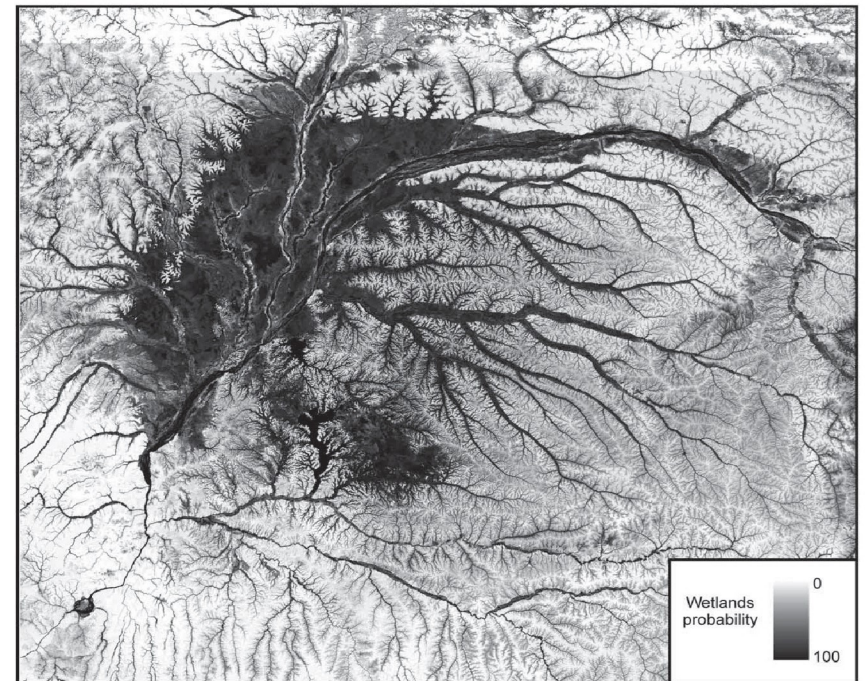
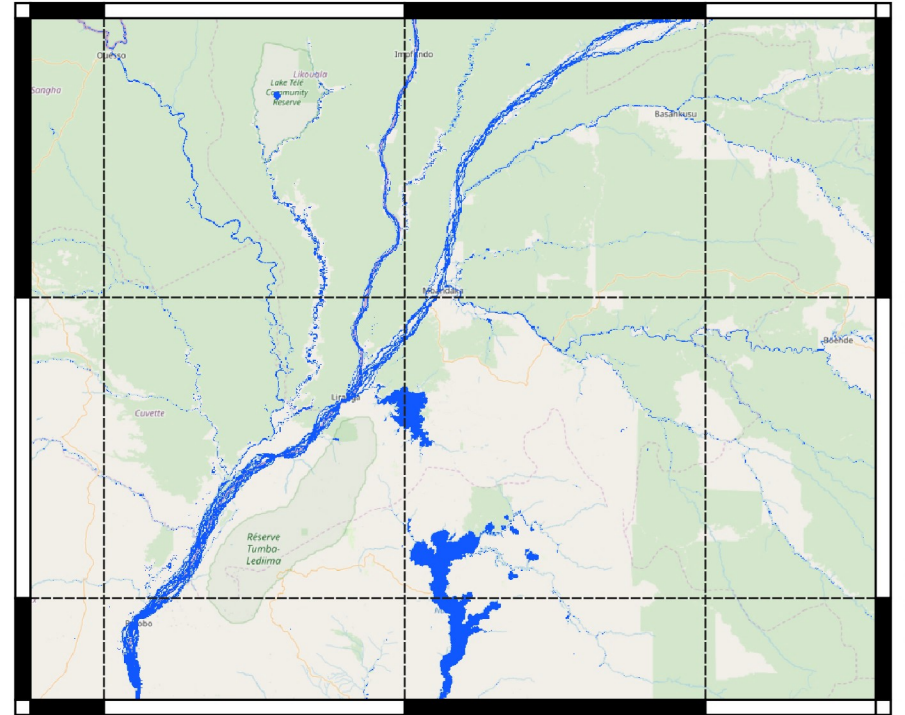
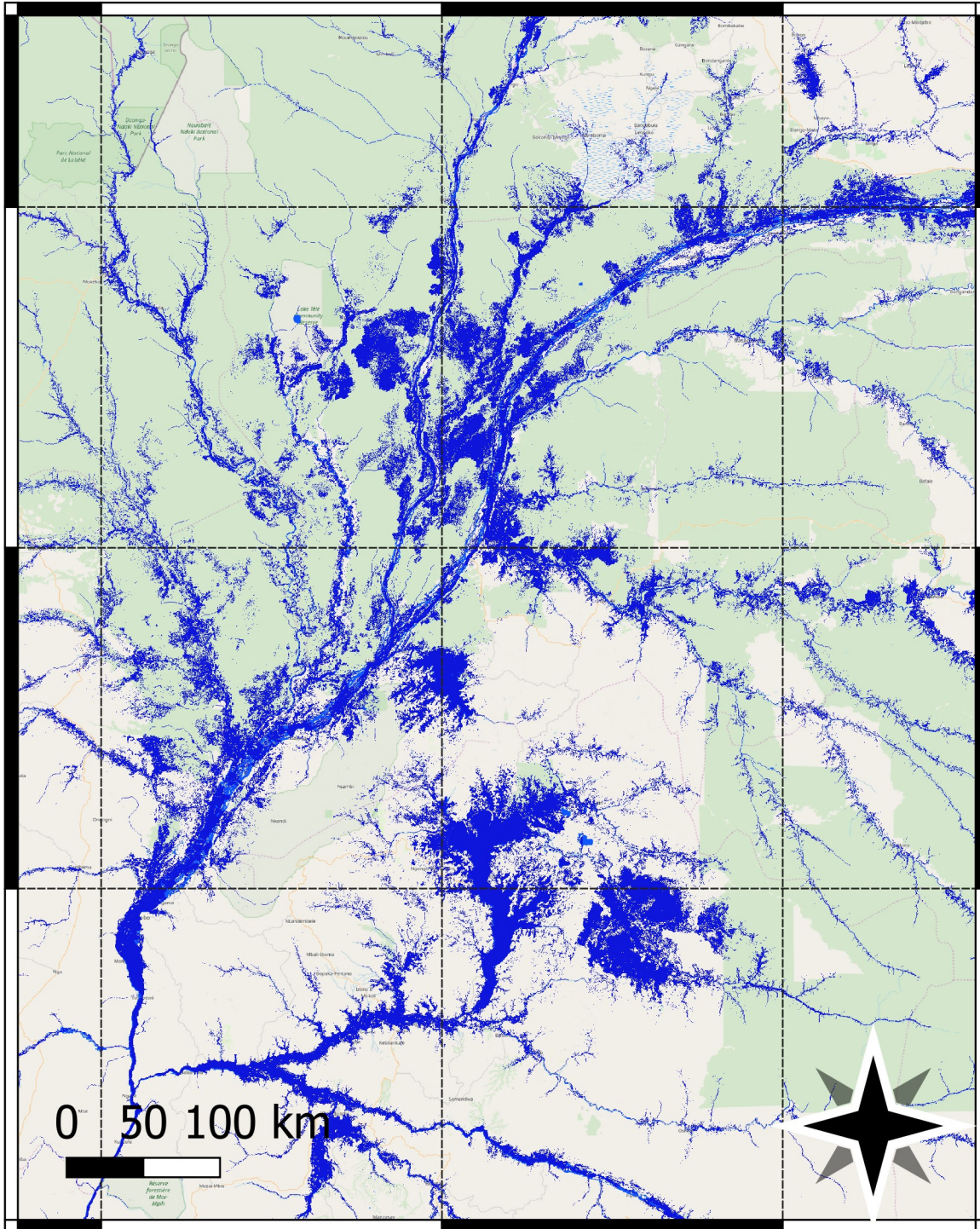
2.000

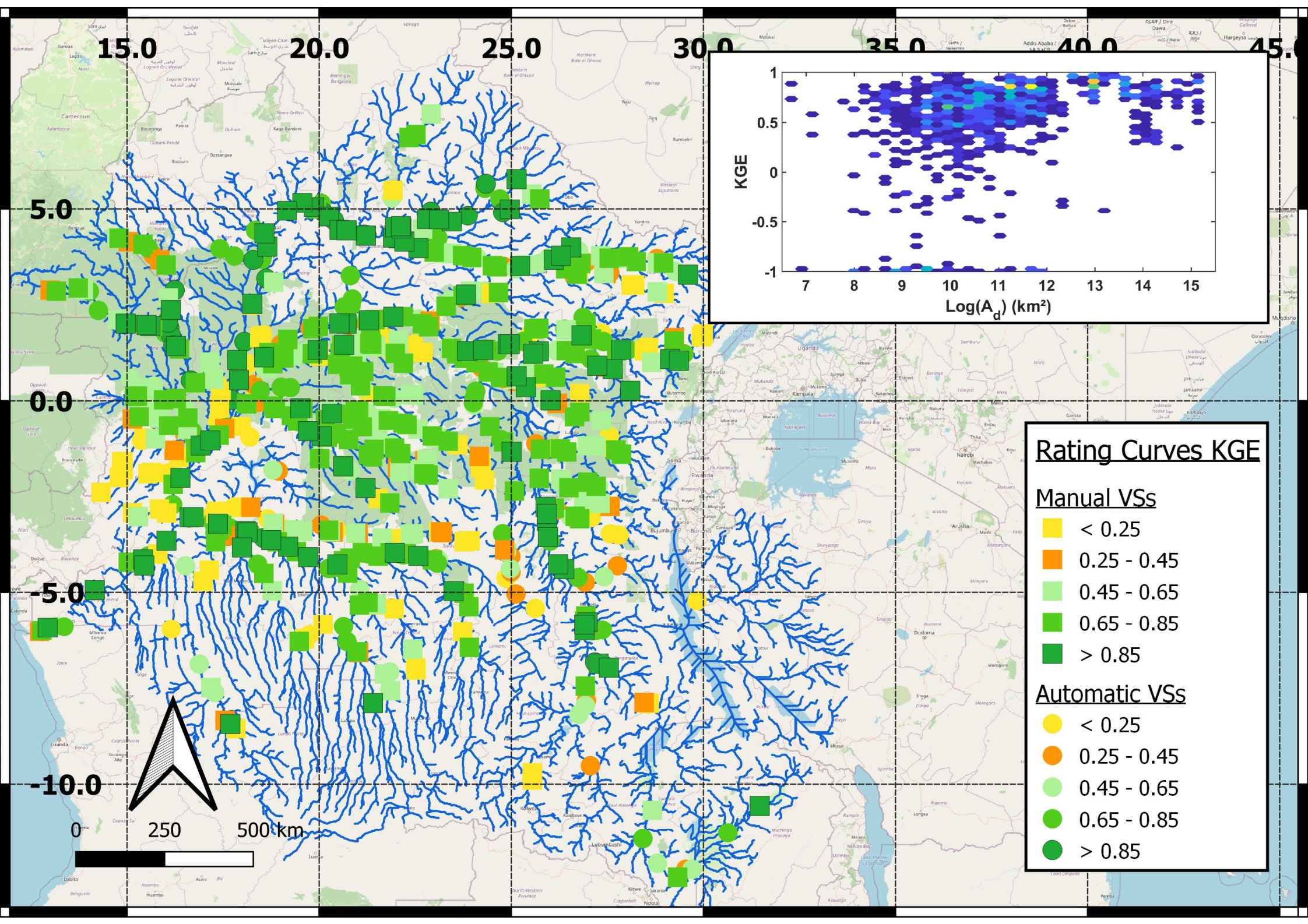
0.000

-2.000

0.000

-2.000





Rating Curves KGE

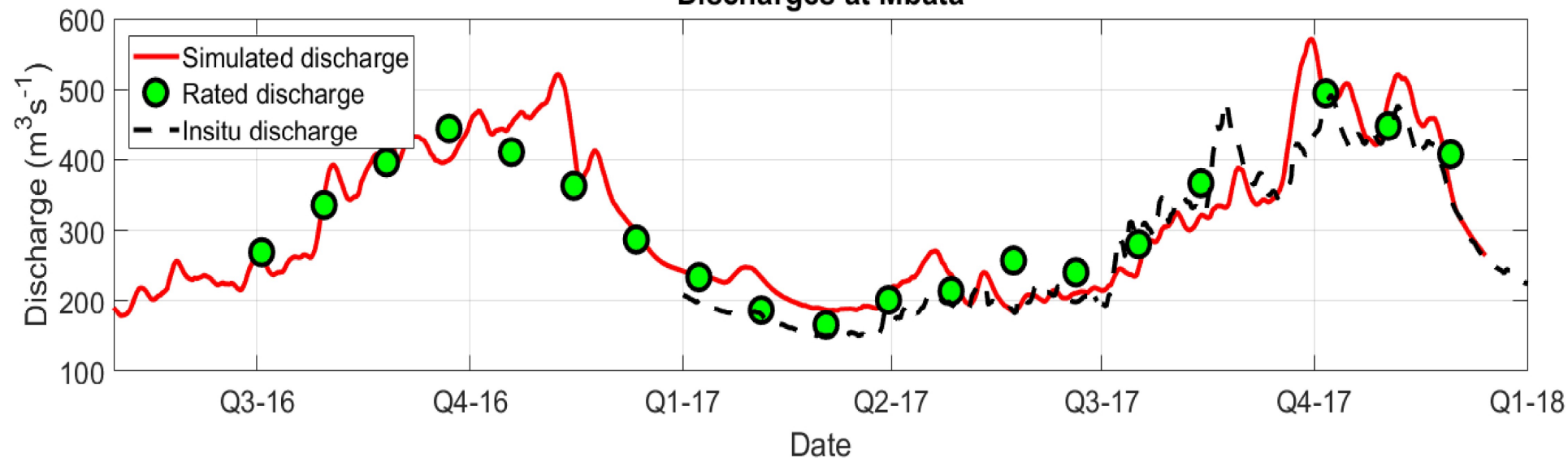
Manual VSs

- < 0.25
- 0.25 - 0.45
- 0.45 - 0.65
- 0.65 - 0.85
- > 0.85

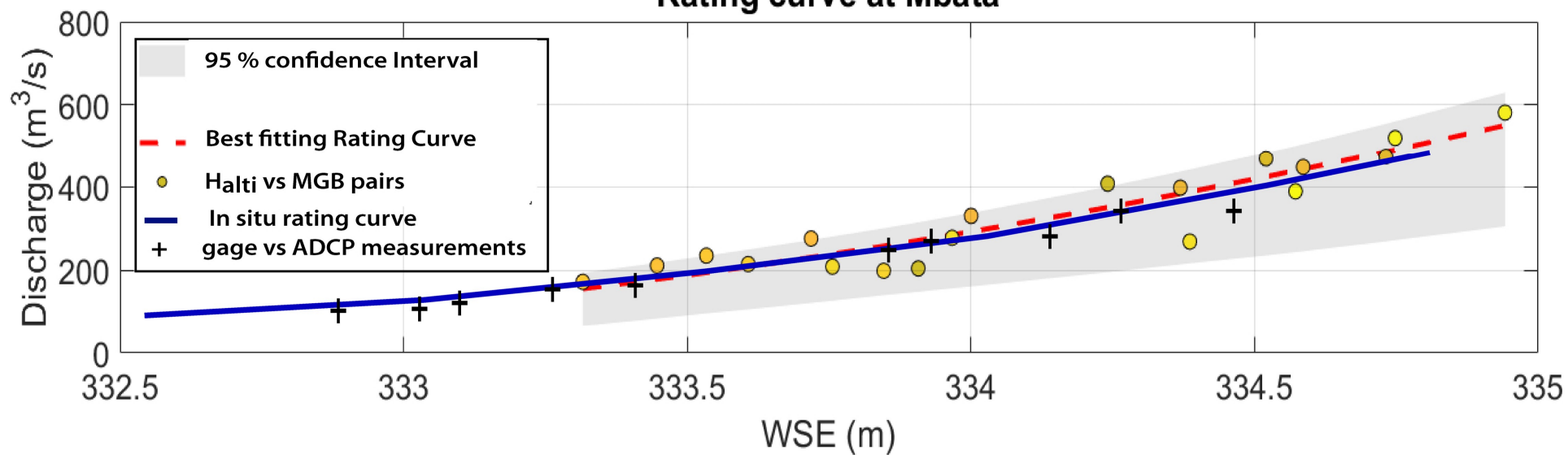
Automatic VSs

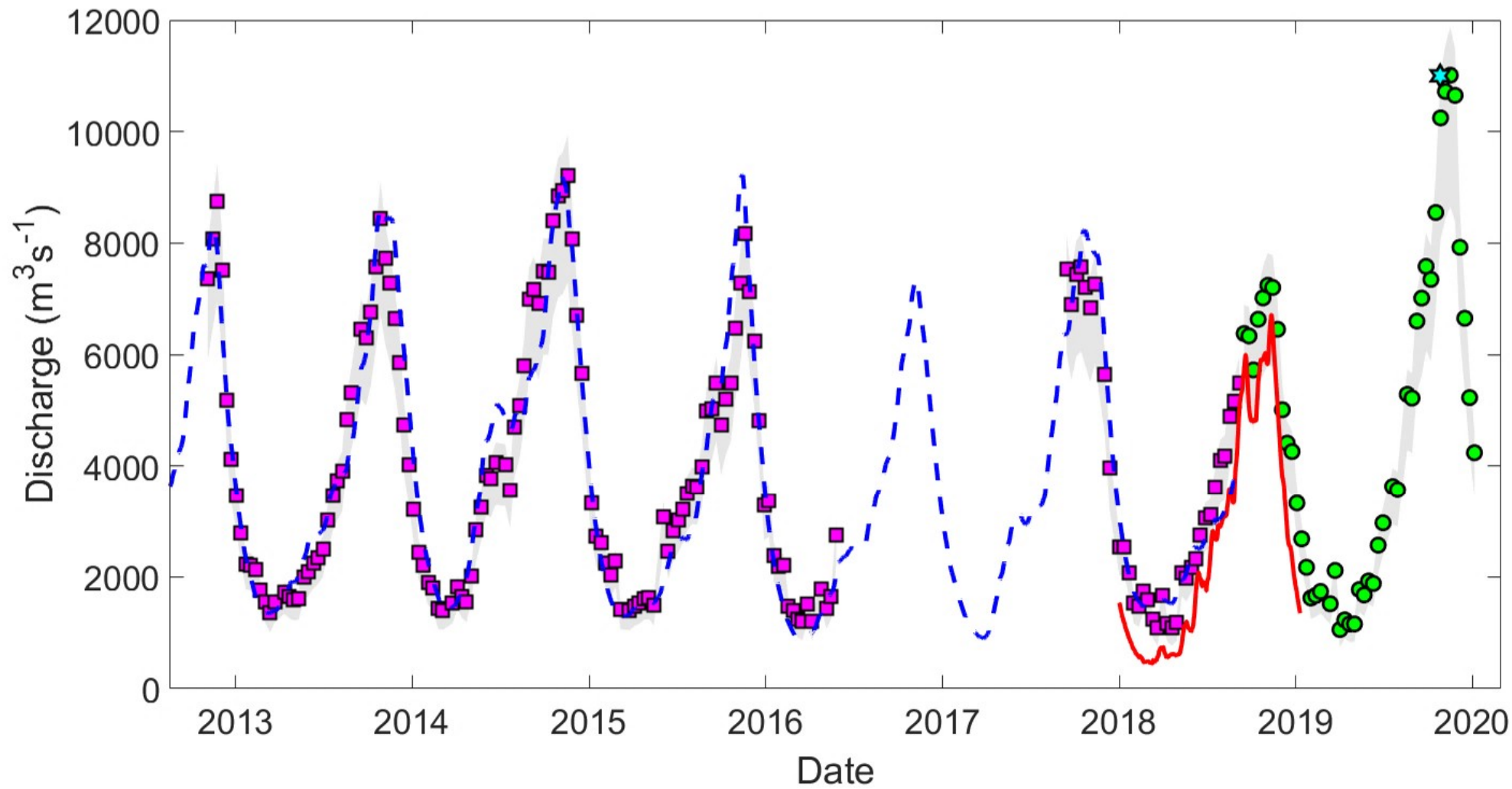
- < 0.25
- 0.25 - 0.45
- 0.45 - 0.65
- 0.65 - 0.85
- > 0.85

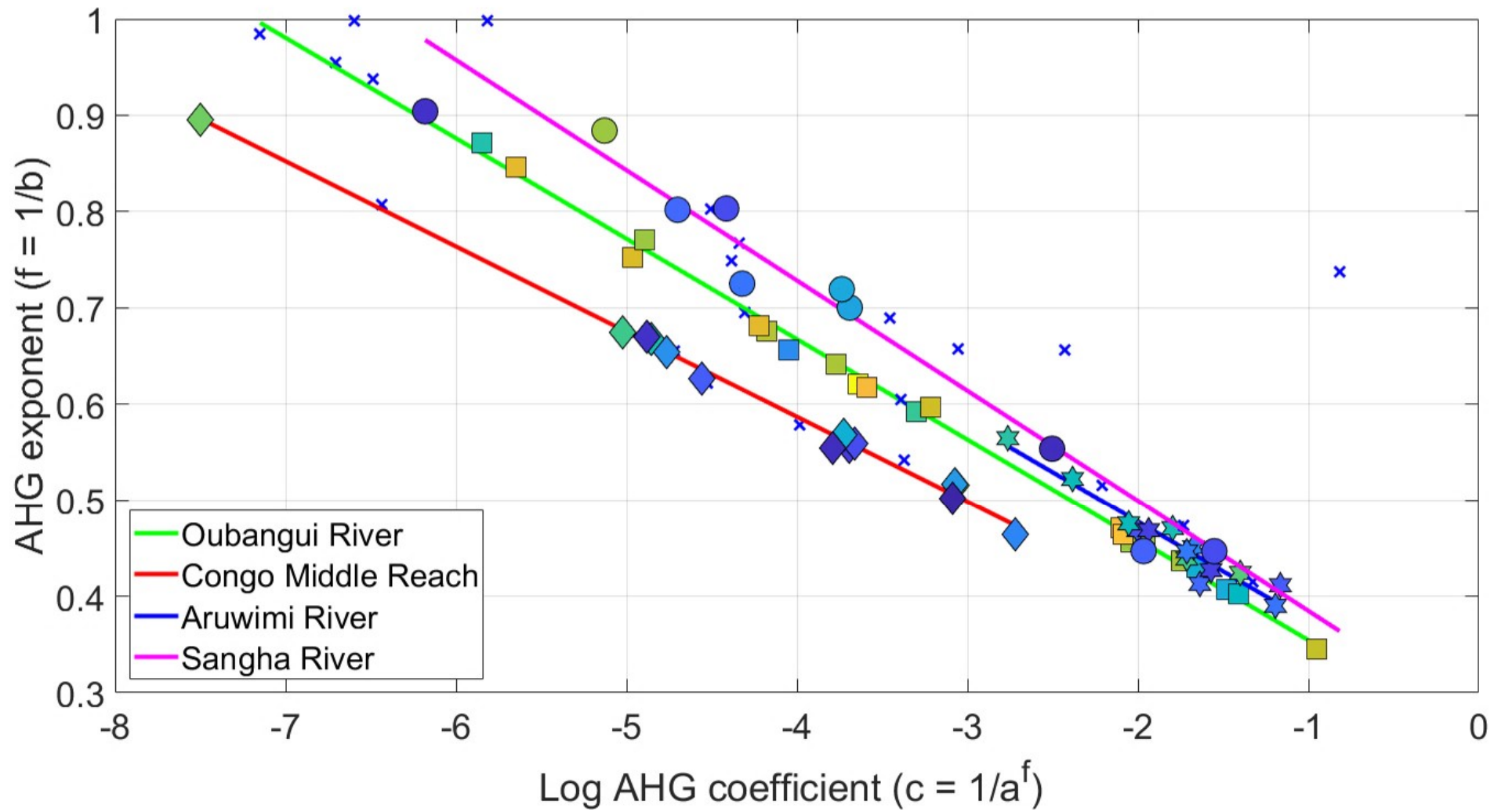
Discharges at Mbata



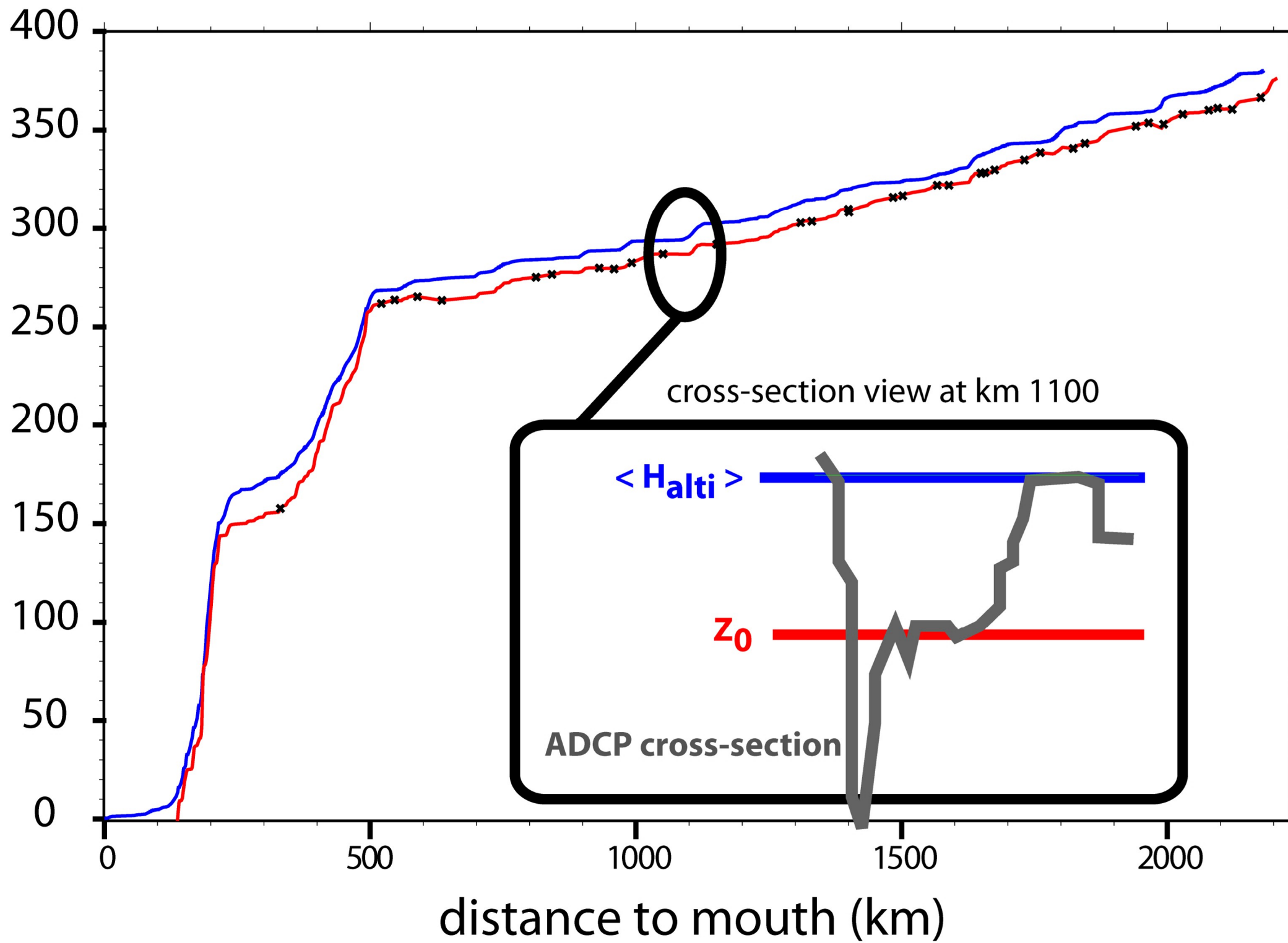
Rating curve at Mbata







Orthometric Height (m)

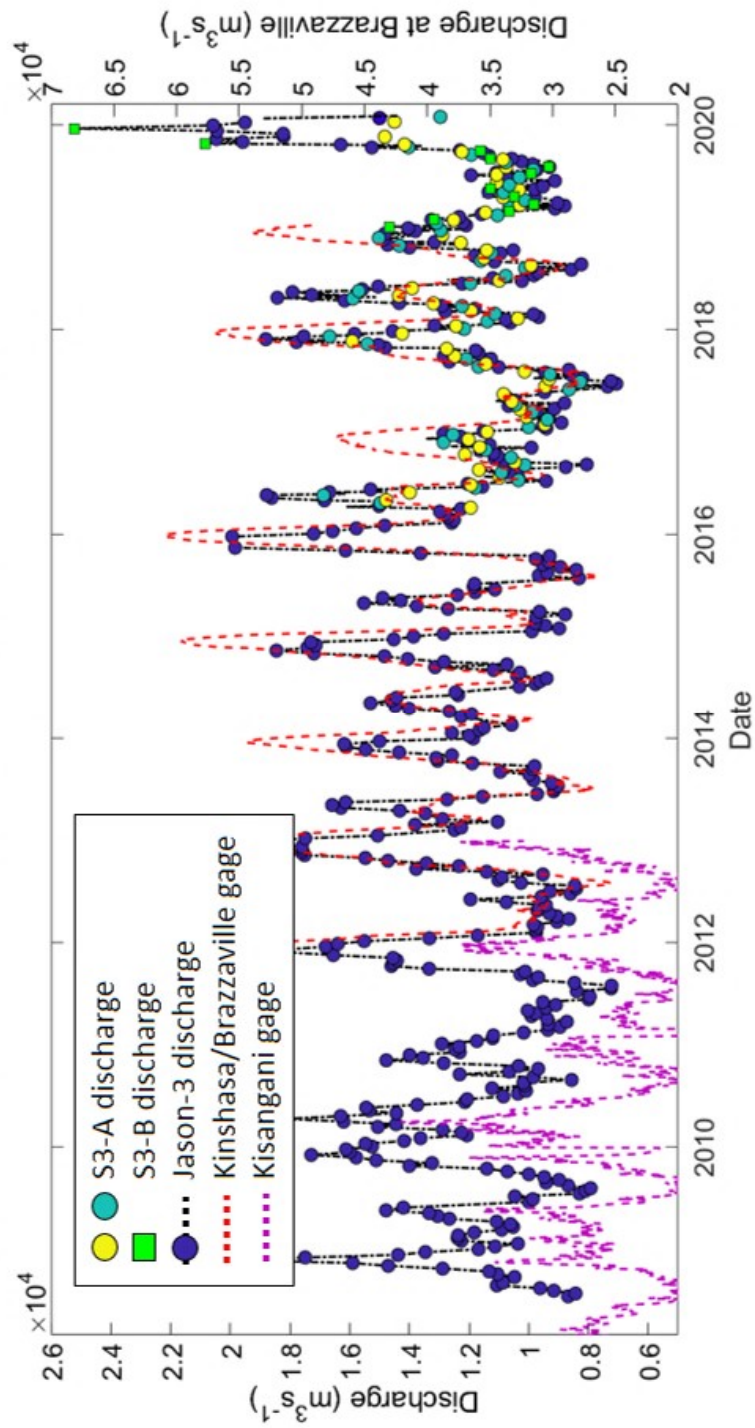
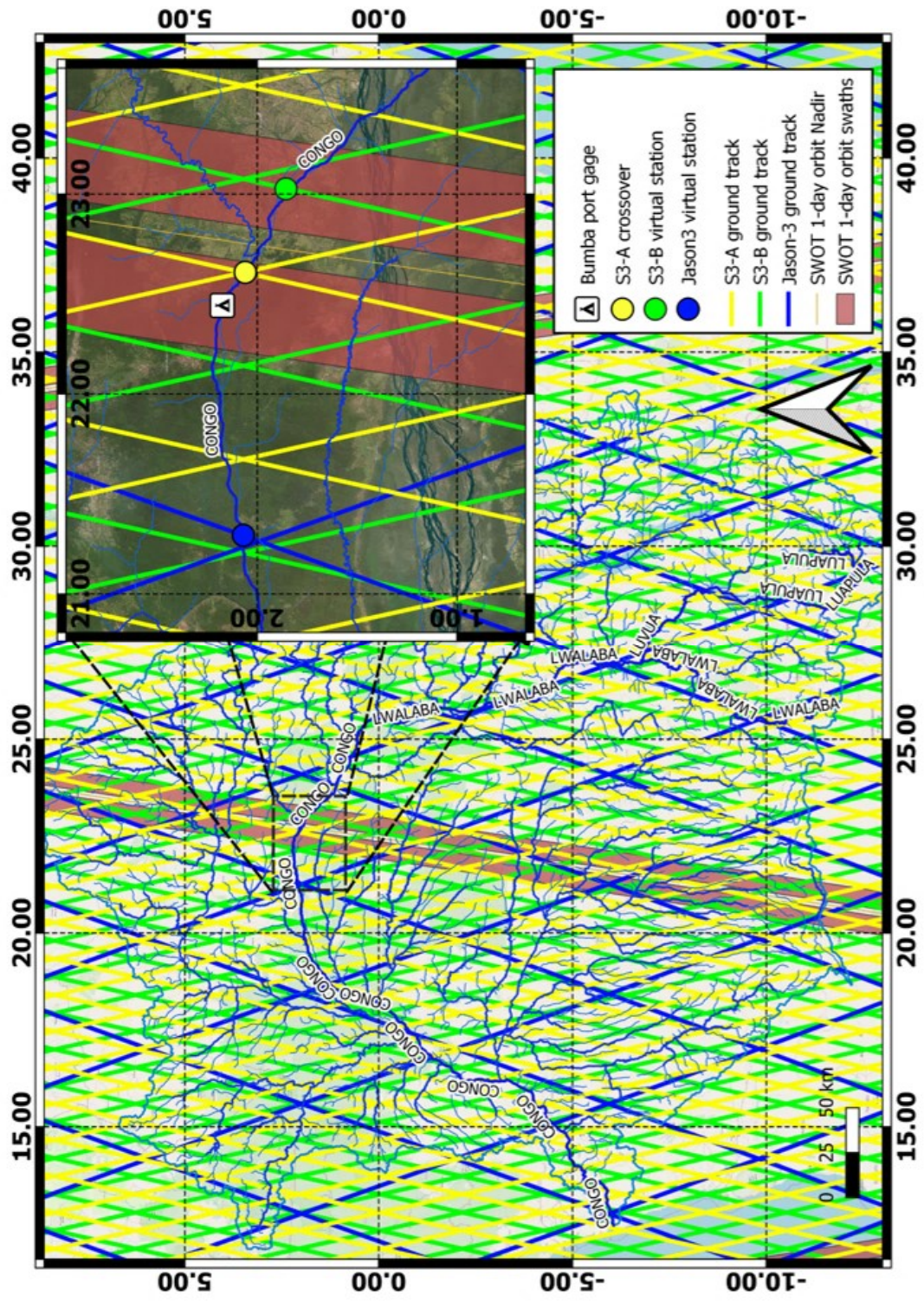


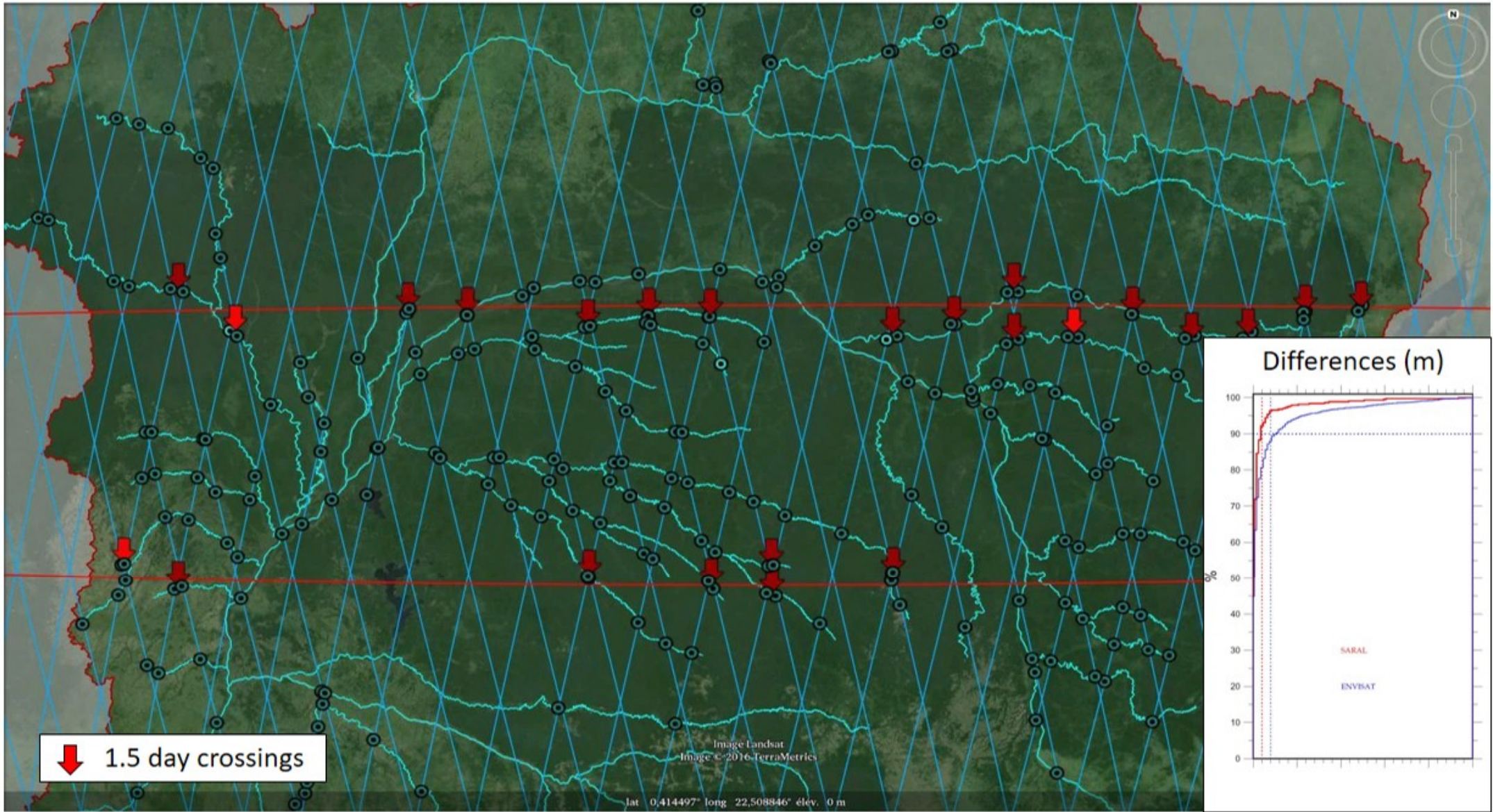
cross-section view at km 1100

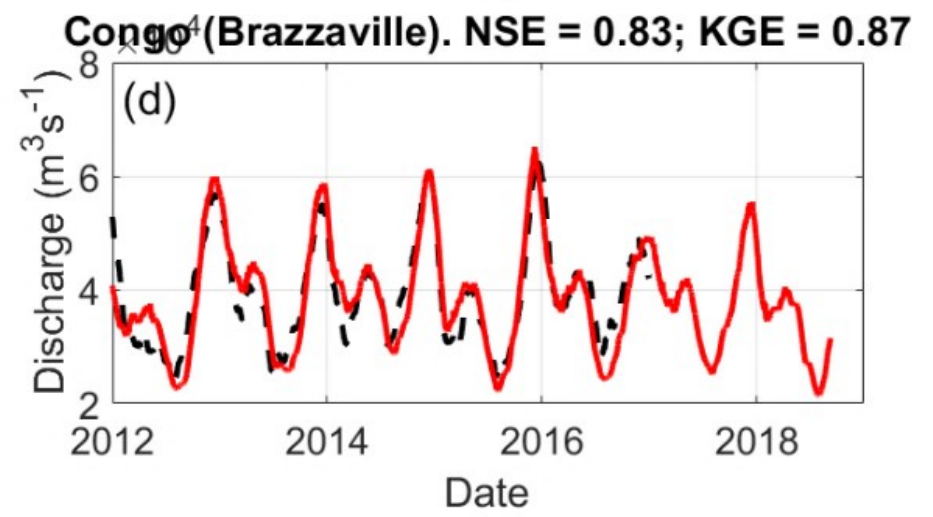
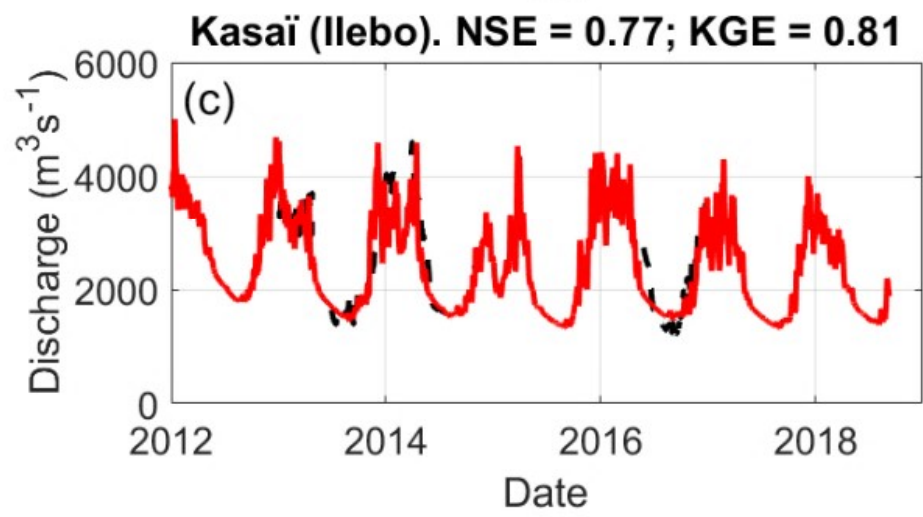
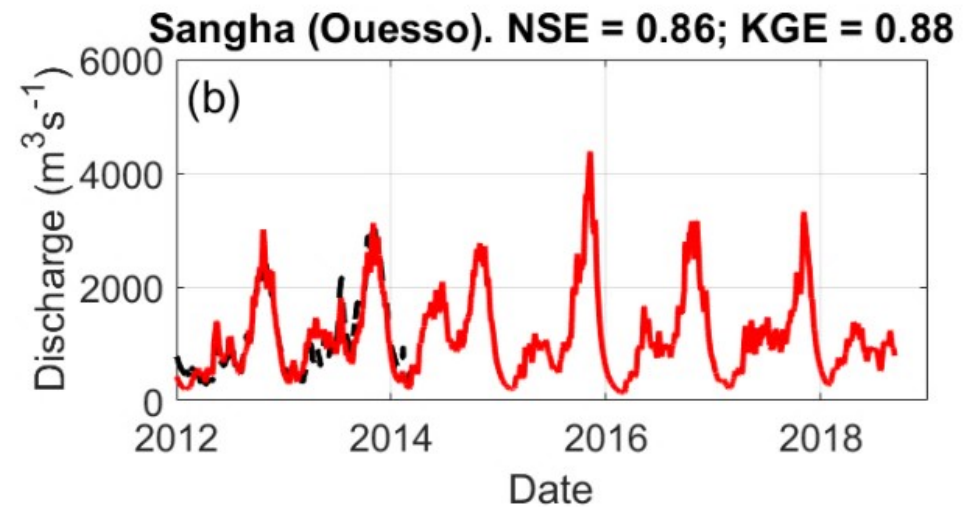
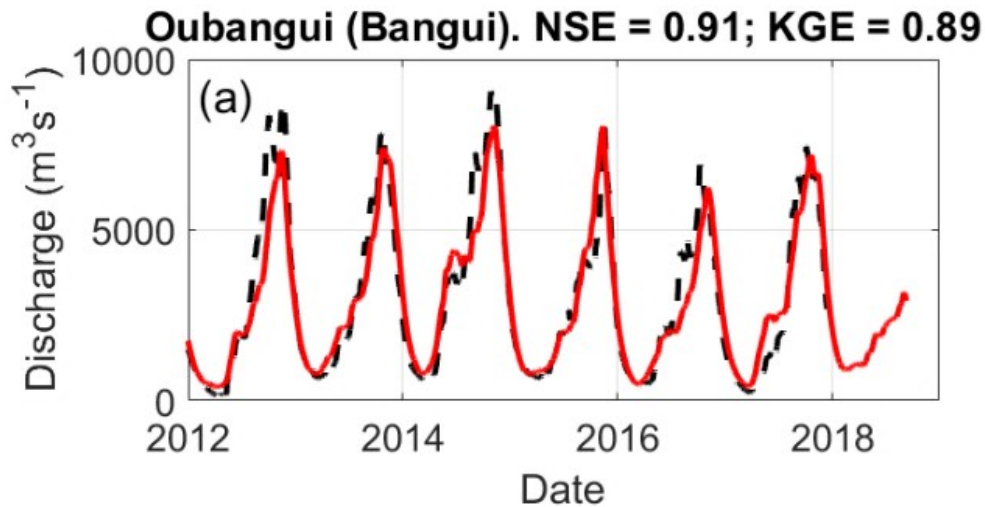
$\langle H_{alti} \rangle$

z_0

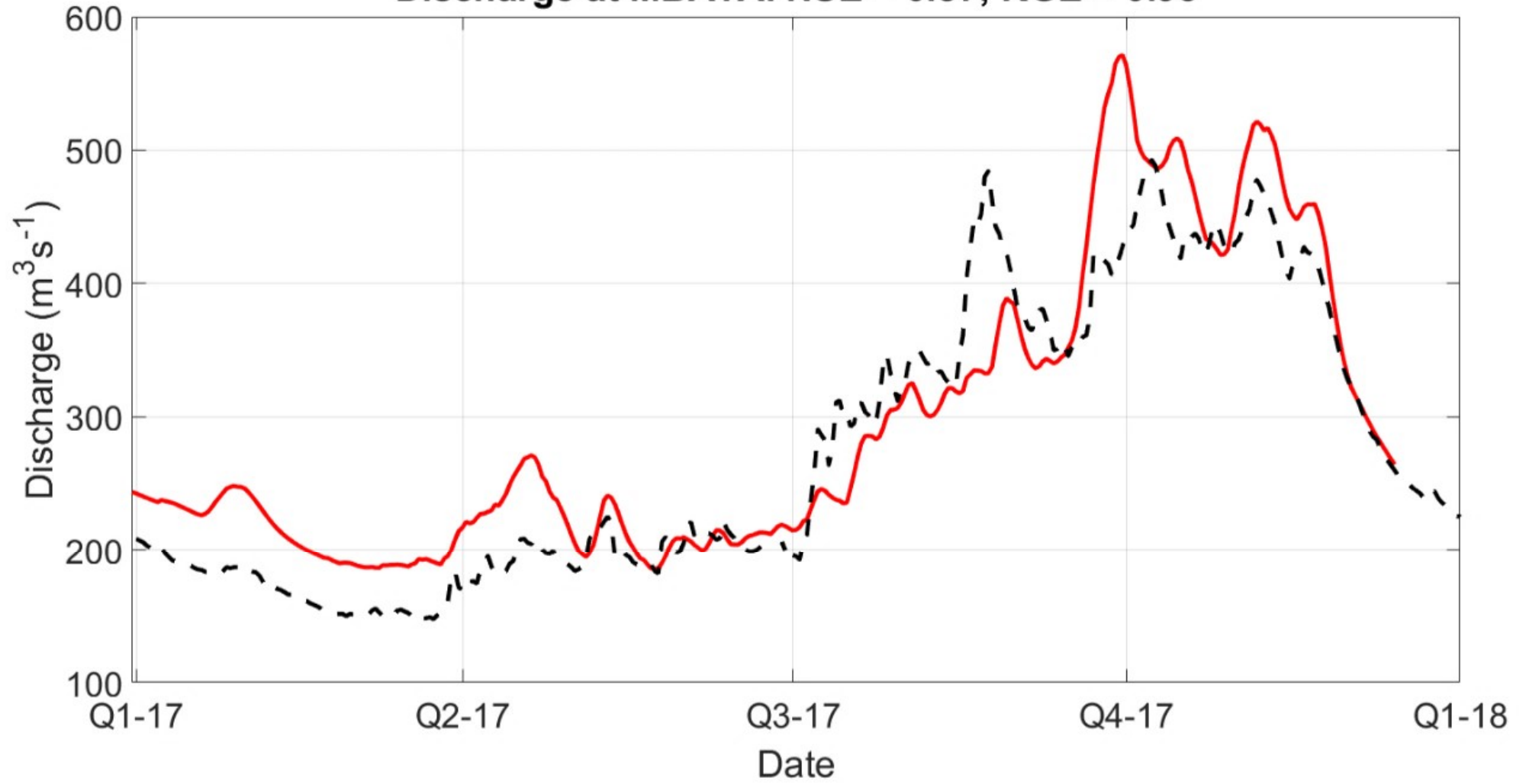
ADCP cross-section

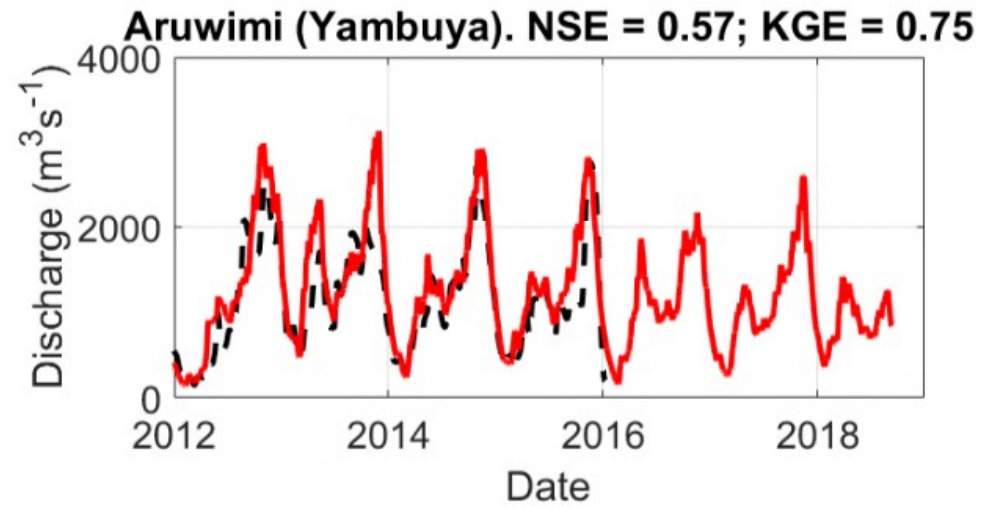
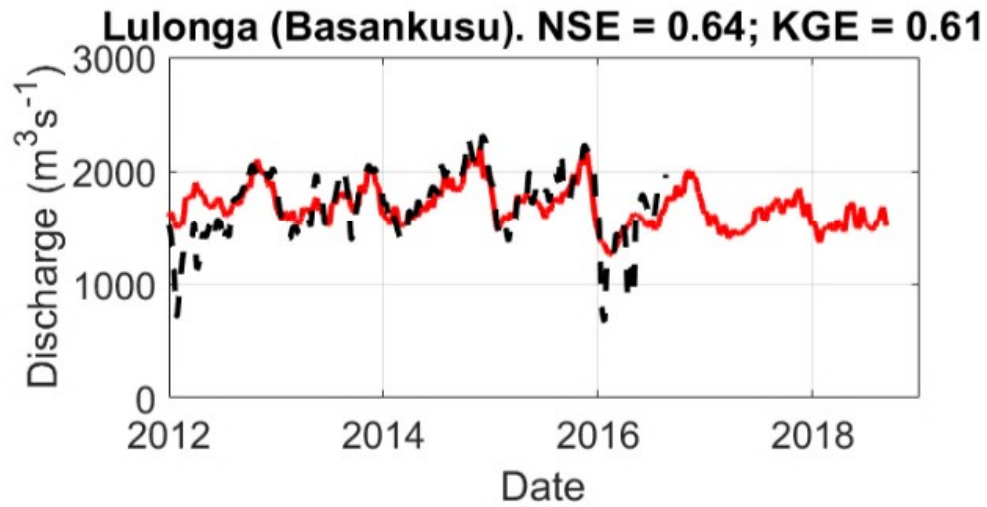
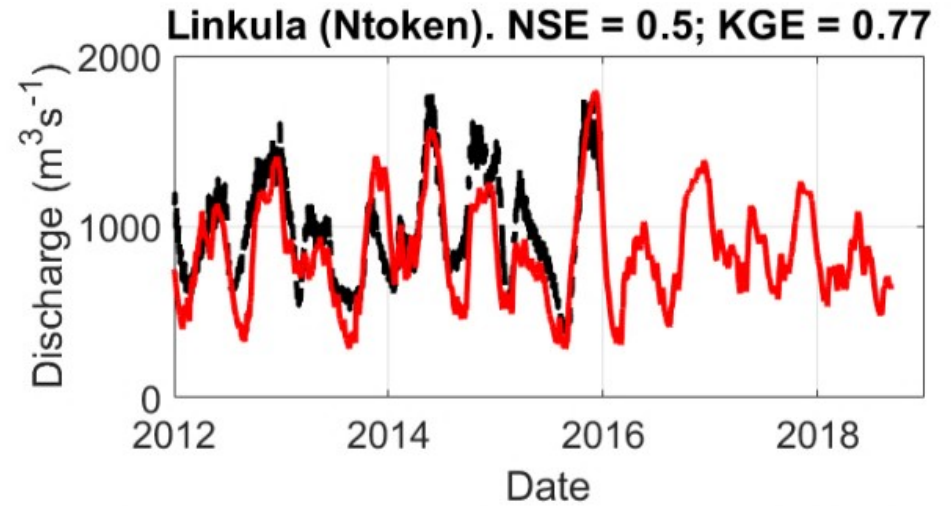
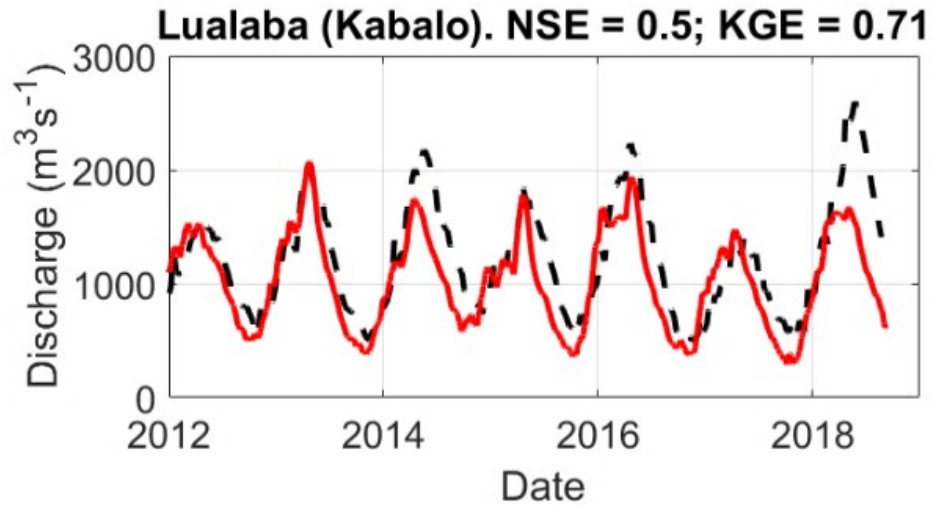


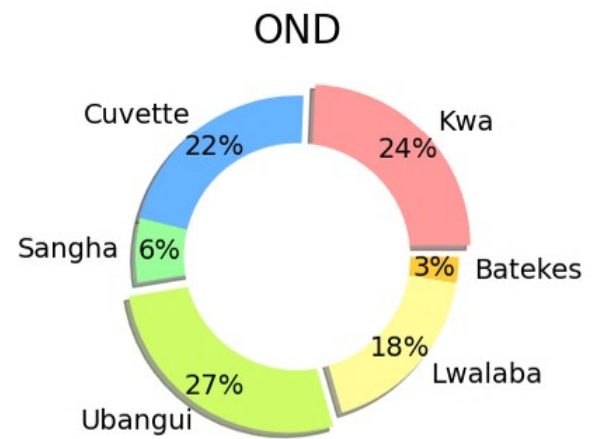
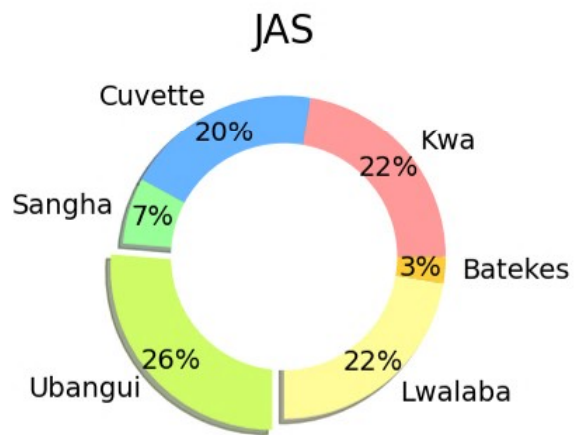
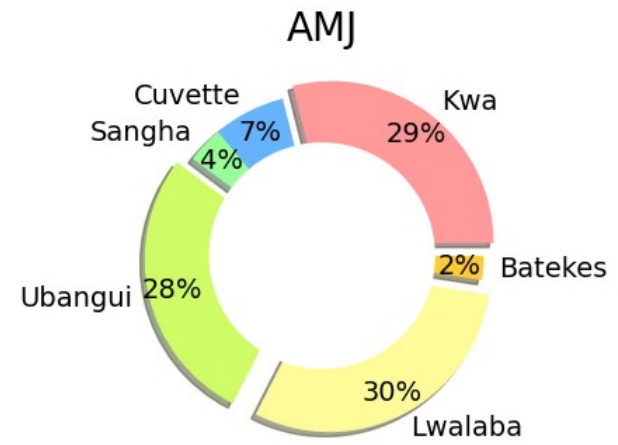
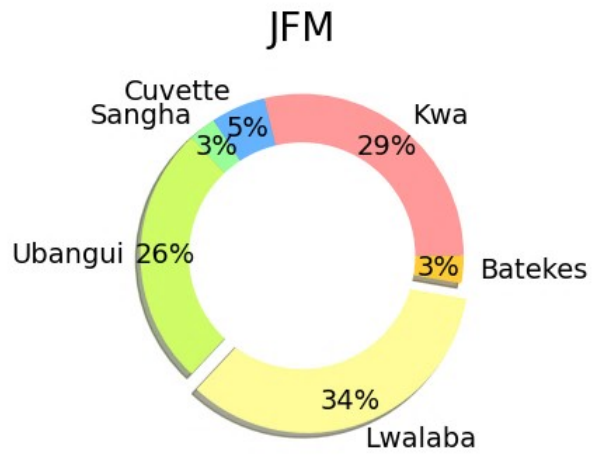




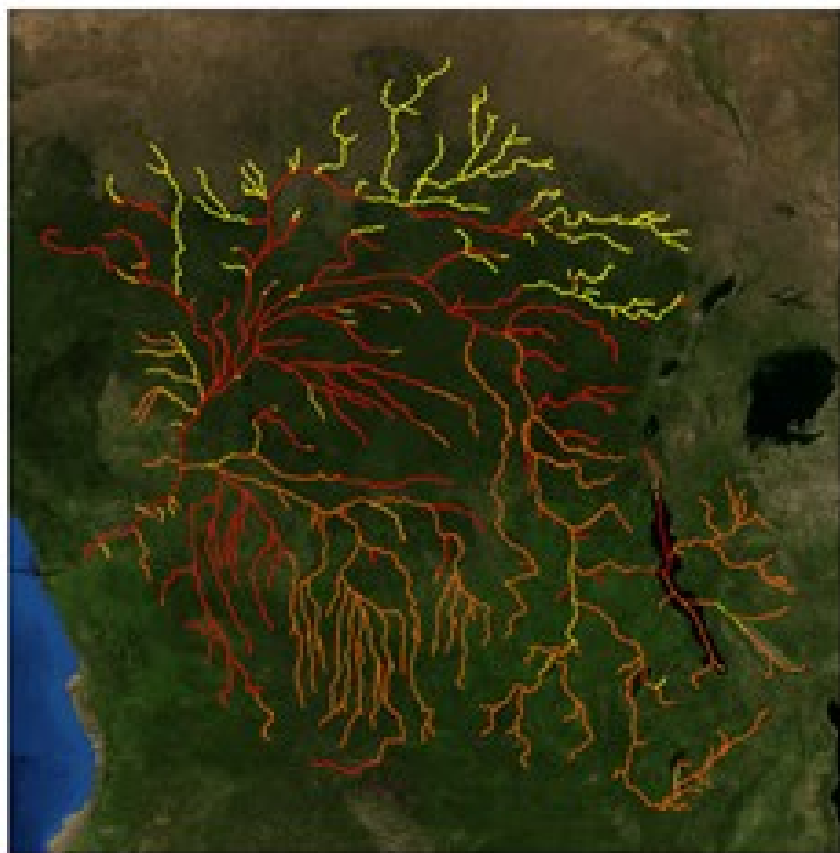
Discharge at MBATA. NSE = 0.87; KGE = 0.93







CRB: trimester of peak flow



CRB: trimester of low flow

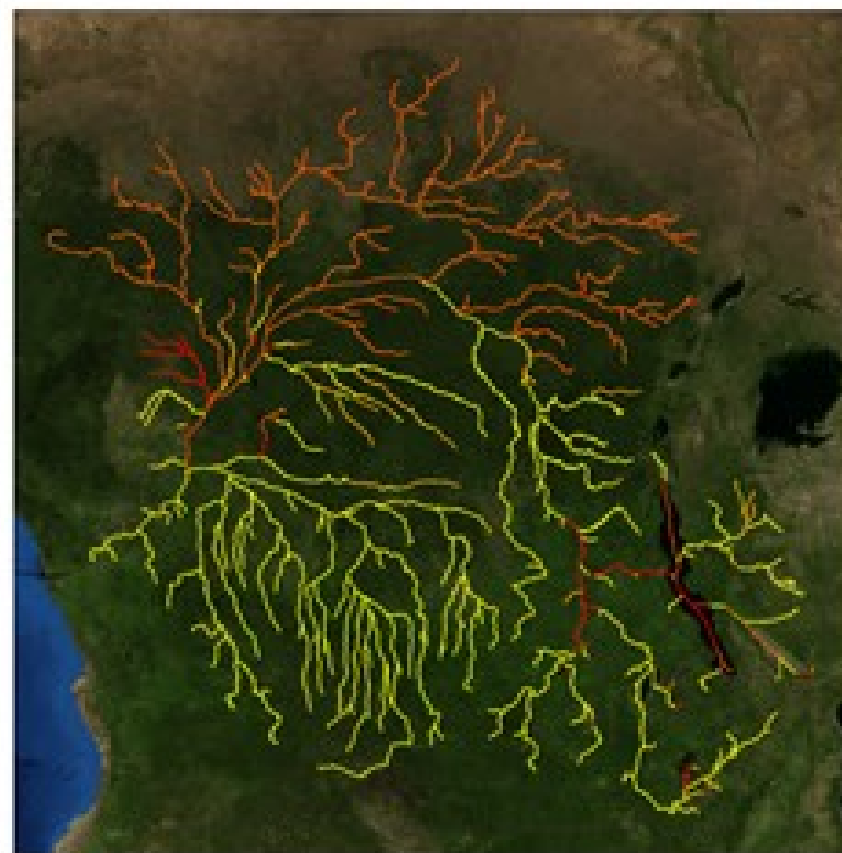


Figure 1: Location of the gages and virtual stations used in this study. Brown square are discharge gages from international databases; Purple triangle is the gage installed at Mbata; Yellow squares are the virtual discharge gages; Red square is the Jason-3 virtual station on the Ubangui River; Violet hexagon is the Sentinel3-B virtual station on the Congo main stem; Blue squares are the operational virtual stations; Green dots are the research virtual stations; The drainage network displayed underneath is extracted through automatic processing part of the DEM using IPH-HydroTools [Siqueira et al., 2016], and the background is from OpenStreetMaps.

Figure 2: (left) mean annual precipitation rate for each catchment (legend provided); (upper right) drainage network extracted from the MERIT DEM (line thickness as a proxy for drainage area; main sub-basins and regions are indicated); (lower right) Hydrological response units (HRUs) as derived from land cover and soil characteristics.

Figure 3: Comparison of simulated discharges with gage discharge from international databases (green dots), gage discharge from recently installed gage (red dot) and virtual discharges (blue dots). Stations names, starting from top upper: Bangui, Ouesso, Ilebo, Brazzaville, Mbata, Kabalo, Ntoken, Basankusu, Yambuya, Ingende, Mulongo, Lediba, Tchepakipa, Bwembe, Kasenga.

Figure 4: Comparison between simulated water levels and satellite altimetry through the ReV indicator.

Figure 5: Comparison between simulated flooded areas (upper panels) and maximum water extent from GSW (lower panels) for the Bangwelu swamps (left) and Upemba wetlands (right).

Figure 6: Focus on the Cuvette Centrale: simulated maximum water extent from MGB (left), maximum water extent from GSW (upper right), and wetland probability from Bwangoy et al. [2010] (lower right).

Figure 7: Distribution of the rating curves extracted for the CRB. Squares are manual VSs, and dots are automatic ones. KGE values nearer from 1 are in green, and yellow is the worst ($KGE < 0.25$); legend is provided. The insert provides the distribution of KGE as a function of drainage area. Density of VSs in the $\text{Log}(Ad)/KGE$ space is represented by a blue-yellow color scale.

Figure 8: Upper panel: discharge at Mbata from different sources (simulated in red, in-situ in black dashed line, and rated in green dots). Lower panel: best fit rating curve at Mbata and its confidence interval between satellite altimetry and simulated discharges (red dashed line

and grey area), with the H/Q pairs (dots). The insitu measurements (black crosses) and rating curve (blue line) are provided.

Figure 9: Discharges from satellite altimetry at VS Ubangui_Jason_248 in the Ubangui River. Purple squares are the rated discharges in MGB run period (i.e. those that are part of the RC); Green dots are discharges estimated from RC with no need of a model run; Red line is the most recent year of data available at Ubangui station –more than 235 km upstream the VS- from the HybAm website; Blue dashed line is the simulated discharge; The blue star is an ADCP measurement performed at Bangui during the flooding event at 2019-10-26. The grey area is the uncertainty bound taken from RC.

Figure 10: Verification of the AMHG log-linear relationship for four rivers in the CRB: the Ubangui River (green line with squares), the Congo middle reach (red line with diamonds), the Sangha River (purple line with dots) and the Aruwimi River (blue line with stars). Best fit linear relationship is identified by solid line, and f/c pairs are identified by symbols. Fill color is the KGE of respective RC (from 0.7 in dark blue to 1 in yellow. Pairs removed by filters (see above) are identified as blue crosses.

Figure 11: Longitudinal profile of the Congo River based on satellite altimetry and MERIT DEM [Yamazaki et al., 2017] as a function of distance to mouth (blue line). The river bed profile is given by the red line. Crosses are the Z0 values at considered VSs. Green line in insert is the cross section as measured by ADCP from CRuHM [2018].

Figure 12: Upper panel: interest points for WSE conversion into discharge from rating curves and AMHG properties. Colored dots are satellite altimetry VSs, the Bumba port is indicated, together with the operational altimetry constellation ground tracks and the SWOT 1-day repeat orbit swaths; Lower panel: discharges of the Congo River from satellite altimetry and AMHG properties. Bright blue and yellow dots are rated discharges at hydroweb S3-A VSs (pass 698 and pass 427 respectively); Green squares are estimated discharges from AMHG properties at S3B VS; Dark blue dots are discharges at nearest downstream Jason-2 and 3 VS (namely pass 070); Purple dashed line is daily discharge at Kisangani (300 km upstream) from CICOS. Red dashed line (right axis) is daily discharge at Brazzaville/Kinshasa from Hybam.

Figure A1: Location of the crossings at 1.5 day apart (red arrow) of the ENVISAT and SARAL virtual stations (blue dots) in the CRB. The ENVISAT ground tracks are indicated in blue lines, and the virtual stations extracted in blue dots. The cumulative distribution of the difference by cycle (1.5 day apart) is presented in the inset, with red curve for the SARAL pairs and the black curve for the ENVISAT pairs

Figure A2: Comparison of climatology (monthly means) from satellite altimetry and gage data. The color code indicates the distance to the gage, negative values stand for cases

where the VS is downstream the gauge and positive values stand for cases where the VS is located upstream the gauge. Grey area is the max/min envelope.

Figure B1: Comparison of in-situ discharge (black dashed line) and simulated discharge (red line) at Bangui (a), Ouesso (b), Ilebo (c) and Brazzaville (d).

Figure B2: Comparison of observed (black dashed line) and simulated (red line) discharge at Mbata (Lobaye River).

Figure B3: Comparison of virtual discharge (black dashed line) and MGB simulated discharge (red line) at Kabalo (Lualaba River, upper left), Ntoken (Linkula River, upper right), Basankusu (Lulonga River, lower left) and Yambuya (Aruwimi River, lower right).

Figure C1: Participation of each zone to the discharge at Kinshasa/Brazzaville, as a function of the trimester. For each period, the major contributor is expanded. When several contributor's contributions lie within 3%, all are expanded.

Figure C2: Spatial distribution of (left) peak flow trimester and (right) low flow trimester. Trimesters were considered as follows: November December January (NDJ); February March April (FMA), May June July (MJJ), and August September October (ASO).